AD-A091 732 OREGON STATE UNIV CORVALLIS AIR RESOURCES CENTER F/G 12/1
AN OBJECTIVE METHOD FOR DETERMINING THE GENERALIZED TRANSPORT. --ETC(U)
AUG 80 E F DANIELSEN, R S HIPSKIND DOT-FA77WA-3992
UNCLASSIFIED FAA/EE-80-32 NL

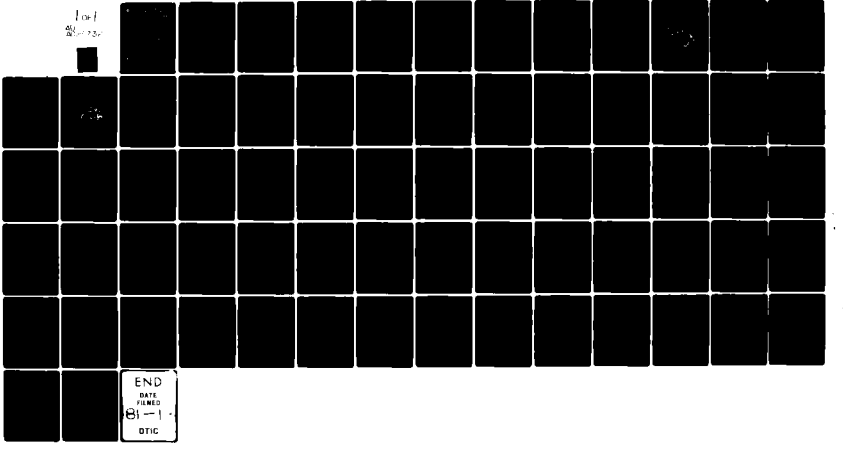

END
DATE FILMED
81-1
DTIC

FAA-EE-80-32

U.S. Department
of Transportation
**Federal Aviation
Administration**

An Objective Method For Determining The Generalized Transport-Tensor For Two-Dimensional Eulerian Models

Office of Environment
and Energy
Washington, D.C. 20591

August 1980

E.F. Danielsen
R.S. Hipskind

Document is available to the public through
the National Technical Information Service,
Springfield, Virginia 22161

(12) FAA/EE

Technical Report Documentation Page

1. Report No. (19) FAA-EE-80-32 ✓	2. Government Accession No.
3. Recipient's Catalog No. (11) 15 Aug 80	
4. Title and Subtitle (6) An Objective Method for Determining the Generalized Transport Tensor for Two-Dimensional Eulerian Models	5. Report Date August 15, 1980
	6. Performing Organization Code (12) 72
7. Author(s) (10) Edwin F. Danielsen and R. S. Hipskind	8. Performing Organization Report No.
9. Performing Organization Name and Address Air Resources Center ✓ Oregon State University Corvallis, Oregon 97331	10. Work Unit No. (TRAIS) (15)
	11. Contract or Grant No. DOT-FA77WA-3992
12. Sponsoring Agency Name and Address U.S. Department of Transportation, Federal Aviation Administration, Office of Environment and Energy, High Altitude Pollution Program Washington, D.C. 20591	13. Type of Report and Period Covered (9) Final Report
	14. Sponsoring Agency Code

15. Supplementary Notes

16. Abstract

An objective method for deriving the components of a generalized transport tensor for a two-dimensional model is presented. The method used representative meridional and vertical velocities and thermodynamic scalars at a uniform grid to reduce the problem to solving two flux equations for two unknowns. One unknown is the stream function, coefficient of an antisymmetric tensor, which corrects the Eulerian mean motions for Stokes drift. The other is a time constant, which converts the deviatory velocity tensor (Reynold's stress tensor for temporal averaging) to a symmetric transport tensor. The complete asymmetric tensor is called a transport rather than a diffusion tensor because its divergence yields both advection and diffusion by the deviatory velocities. Advantages and disadvantages of Lagrangian and Eulerian averages are also discussed.

17. Key Words	18. Distribution Statement
2-D Model, Transport tensor, Diffusion, Mean motions, Eulerian and Lagrangian reference, Stokes drift.	Available to the public through National Technical Information Service, Springfield, Virginia 22161.

19. Security Classif. (of this report)	20. Security Classif. (of this page)	21. No. of Pages	22. Price
Unclassified	Unclassified	65	

Form DOT F 1700.7 (8-72) Reproduction of completed page authorized

New 4/2c35

AN OBJECTIVE METHOD FOR DETERMINING THE GENERALIZED TRANSPORT TENSOR FOR TWO-DIMENSIONAL EULERIAN MODELS

Edwin F. Danielsen
and
R. S. Hipskind

Air Resources Center
Oregon State University
Corvallis, Oregon

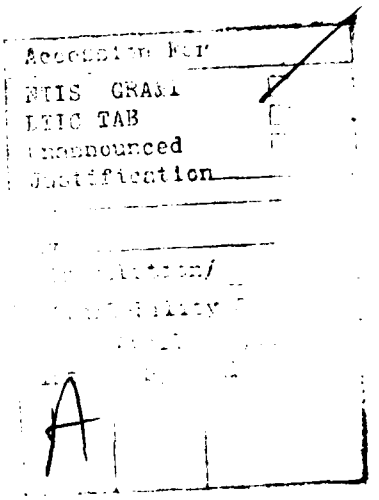

ABSTRACT

An objective method for deriving the components of a generalized transport tensor for a two-dimensional model is presented. The method used representative meridional and vertical velocities and thermodynamic scalars at a uniform grid to reduce the problem to solving two flux equations for two unknowns. One unknown is the stream function, coefficient of an antisymmetric tensor, which corrects the Eulerian mean motions for Stokes drift. The other is a time constant, which converts the deviatory velocity tensor (Reynold's stress tensor for temporal averaging) to a symmetric transport tensor. The complete asymmetric tensor is called a transport rather than a diffusion tensor because its divergence yields both advection and diffusion by the deviatory velocities. Advantages and disadvantages of Lagrangian and Eulerian averages are also discussed.

CONTENTS

INTRODUCTION

Atmospheric transport of trace species is a very controversial and conceptually difficult subject despite the fact that only two processes are involved: transport by mean motions and by deviations from the means. (Here the latter are called deviatory motions.) This partitioning of the transport is necessary for any model, whether conceptual, analytical or numerical, having more than one independent spatial variable, because the complete transport cannot be resolved deterministically. For example, in a 3-D model the size of the averaging volume is primarily limited by the observations themselves. All effects of velocities which cannot be observed must be described statistically via subgrid scale parameterizations. Increasing the averaging volume to include all longitudes yields the conventional 2-D meridional-height model, although one could integrate over all latitudes to produce a longitudinal-height model.

In either case, the local mean motions which are resolved in a 3-D model, contribute to both mean and deviatory motions in a 2-D model. If we restrict discussion to zonally averaged models, a Fourier analysis of the 3-D local-mean velocities includes the zonal-mean velocities as wave number zero, while all non-zero wave numbers contribute to the deviatory motions. In other words, the classification of all non-zero wave numbers switches by the elimination of one spatial dimension.

The switch in classification is not trivial, however, because it implies a change from a known variable, either measured or predicted, to an unknown whose effects must be described statistically. In principle, the description could be rather simple and straightforward if the observations were not so severely limited. In fact, the limitations make it very difficult to obtain reliable or representative statistics and, consequently, there has been considerable subjectivity in their description, and controversy about the methods

used to parameterize their effects.

OPEN EULERIAN SYSTEMS VERSUS SEMICLOSED LAGRANGIAN SYSTEMS

The earth's atmosphere is strongly anisotropic with typical horizontal length scales 500 to 1000 times the vertical scales. Consistent with this dimensional asymmetry, the large-scale waves which dominate the transport have horizontal speeds of tens of meters per second and vertical speeds of centimeters per second. These vertical speeds are too small to be measured by any conventional in situ or remote sensors, so, by observational default, the large-scale waves appear to be two-dimensional. But, if one considers the atmosphere's anisotropy, it becomes clear that small vertical speeds are as effective to vertical transport as are large horizontal speeds to horizontal transport. The velocities and distances are similarly scaled.

Given the observational limitations, that only horizontal velocities can be measured and that only the large-scale winds can be resolved, we are forced to compute the associated large-scale vertical velocities from the equations of fluid dynamics, appropriately modified to apply to large bulk systems. The fundamental equations are derived for small elemental volumes, say 1 mm^3 or 1 cm^3. But, for global or hemispheric atmospheric analyses, we must use bulk volumes of 10^{19} or $10^{20} cm^3$.

The volumes used in 2-D models average about $10^{22} cm^3$. A 10% increase in the exponent of the integration volume hardly seems dramatic, but its' effects on our concepts of transport are potentially confusing because, as mentioned earlier, all of the large-scale waves vanish in the integration. Contributing to the confusion is a current controversy over the type of integration to use for evaluating 2-D model parameterizations. Recently it has become fashionable to claim that Eulerian integrals, with their competitive component

terms, are inherently ambiguous; only Lagrangian integrals should be used. Implicit in these claims - sometimes it is even stated explicitly - is the attractive but realistically unattainable assumption that Lagrangian integrals eliminate all deviatory motions, i.e., that they describe closed systems.

To demonstrate that closed systems are idealizations for either 2 or 3-D models, let us consider 1 cm^3 as a reasonable elemental volume and a bulk system containing 10^{20} elemental volumes. For a closed system the following constraint must hold. If V is the velocity of an elemental volume and V_B is the velocity of the boundary surface, then V must equal V_B at all points on the boundary. Although the velocities of the elemental volumes are not completely independent of each other their differences over the surface of the bulk volume are large, therefore, the bulk volumes rapidly deform. Most importantly, it is impossible to determine subsequent positions of an initially prescribed boundary.

A more reasonable constraint for a Lagrangian integral, an extension of the molecular constraint for an elemental system, is to consider a bulk, open system whose integrated, deviatory mass flux across the boundary surface is zero (see Appendix I for details). With this constraint the bulk system conserves its total mass, moves with the mean velocity, the velocity of its center of mass, and deforms due to spatial gradients of these same mean velocities. Therefore, in principle, one can determine both the movement of the center of mass and the boundaries of each bulk system knowing only the mean velocities. However, the deviatory velocities of the Lagrangian integrals remain unknown for the same reason that they are unknown with Eulerian integrals.

Consequently, the distinction between Eulerian and Lagrangian integrals and their associated means is not that of an open versus a closed system; rather it is one of a stationary, completely open system versus a moving, partially

closed system. The degree of closure depends directly on the size of the bulk system which, in turn, depends upon the resolution limits imposed by the data or by the computer.

THREE-DIMENSIONAL TRANSPORT BASED ON QUASI-LAGRANGIAN TRAJECTORIES

For a 3-D diagnostic or predictive model, the use of Lagrangian integrals is equivalent to generating three-dimensional trajectories which trace out the motion of the center of mass of the bulk systems. On the other hand, Eulerian integrals yield a succession of streamline (or the associated stream function and velocity potential) analyses. If the grid volumes of both integrals are comparable in size the trajectories and the streamlines describe the same local mean motions but from different viewpoints. Although a complete description would yield the same results, one's subjective concepts of the transport could be considerably different for the two systems.

The streamline analyses tend to emphasize wave motions and laminar-like flow, while the trajectories emphasize dispersion and turbulent-like flow. The latter can be seen in Fig 1 which resembles a plate of tangled spaghetti. Actually, it represents 80 to 160 isentropic trajectories which were calculated by a computer using programs based on the methods developed by Danielsen (1961; 1967). Analyses of the isentropic stream function over the northern hemisphere, north of 20^{o}N, were made by hand. After gridpoint values were read, coded and verified the balance equation was solved for an ageostrophic stream function. Then trajectories were computed from the ageostrophic winds.

These trajectories have been designated here as quasi-Lagrangian because they were based on the isentropic approximation and because the contributions from a velocity potential were neglected. Thus, the effects of deviatory boundary fluxes were not included in the trajectory computations and no attempt

Fig 1. Isentropic trajectories, objectively computed on θ = 310K surface. Initial points correspond to odd numbered gridpoints of Fig 2a, 0000 GMT, 18 April 1963. Final points for trajectories which remain inside grid are plotted in Fig 2b, 1200 GMT, 24 April 1963. Trajectories leaving grid are terminated as they approach 20^{o}N latitude.

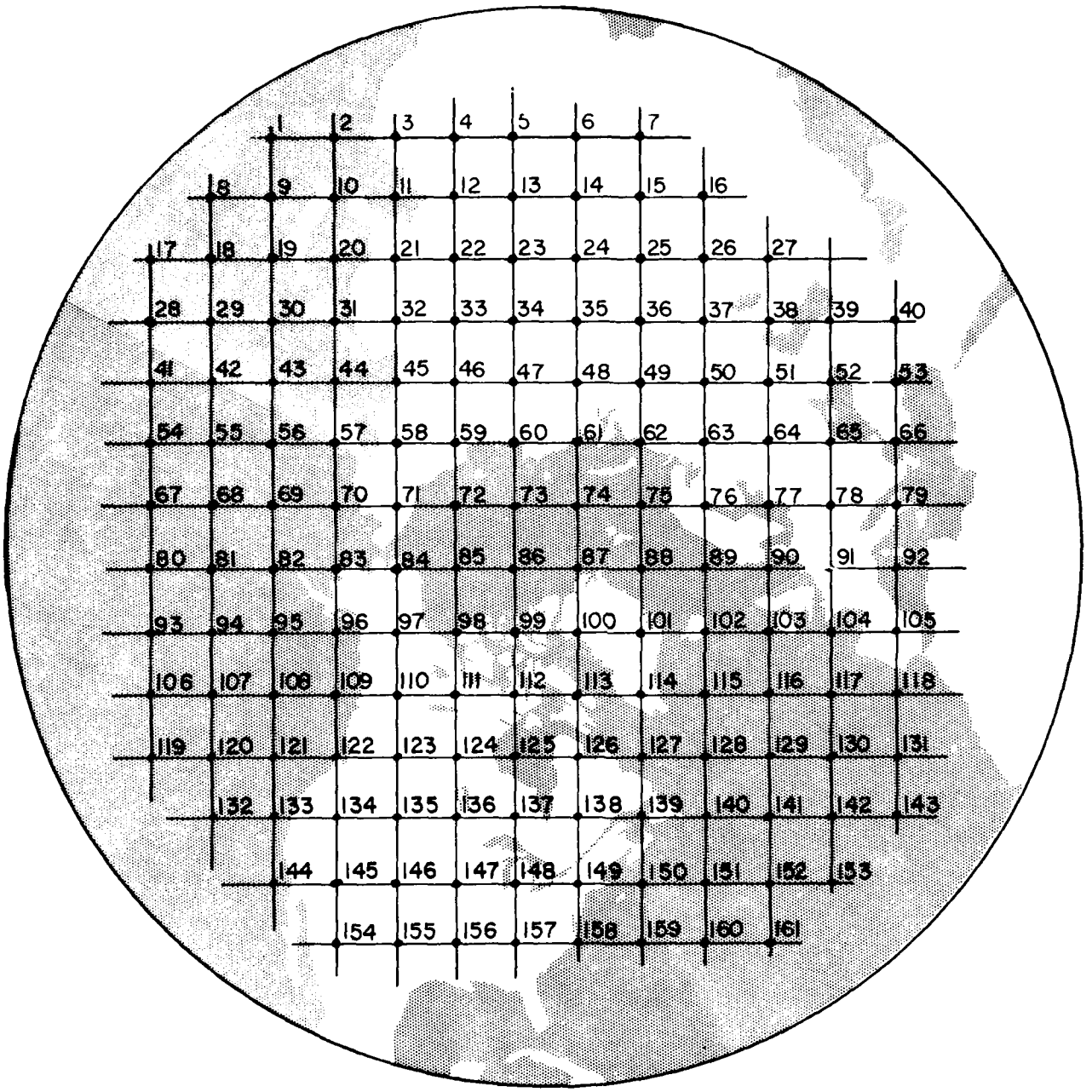

Fig 2a. Initial gripdoints for trajectory computations. Note the trajectories in Fig 1 originate at only the odd numbered gridpoints.

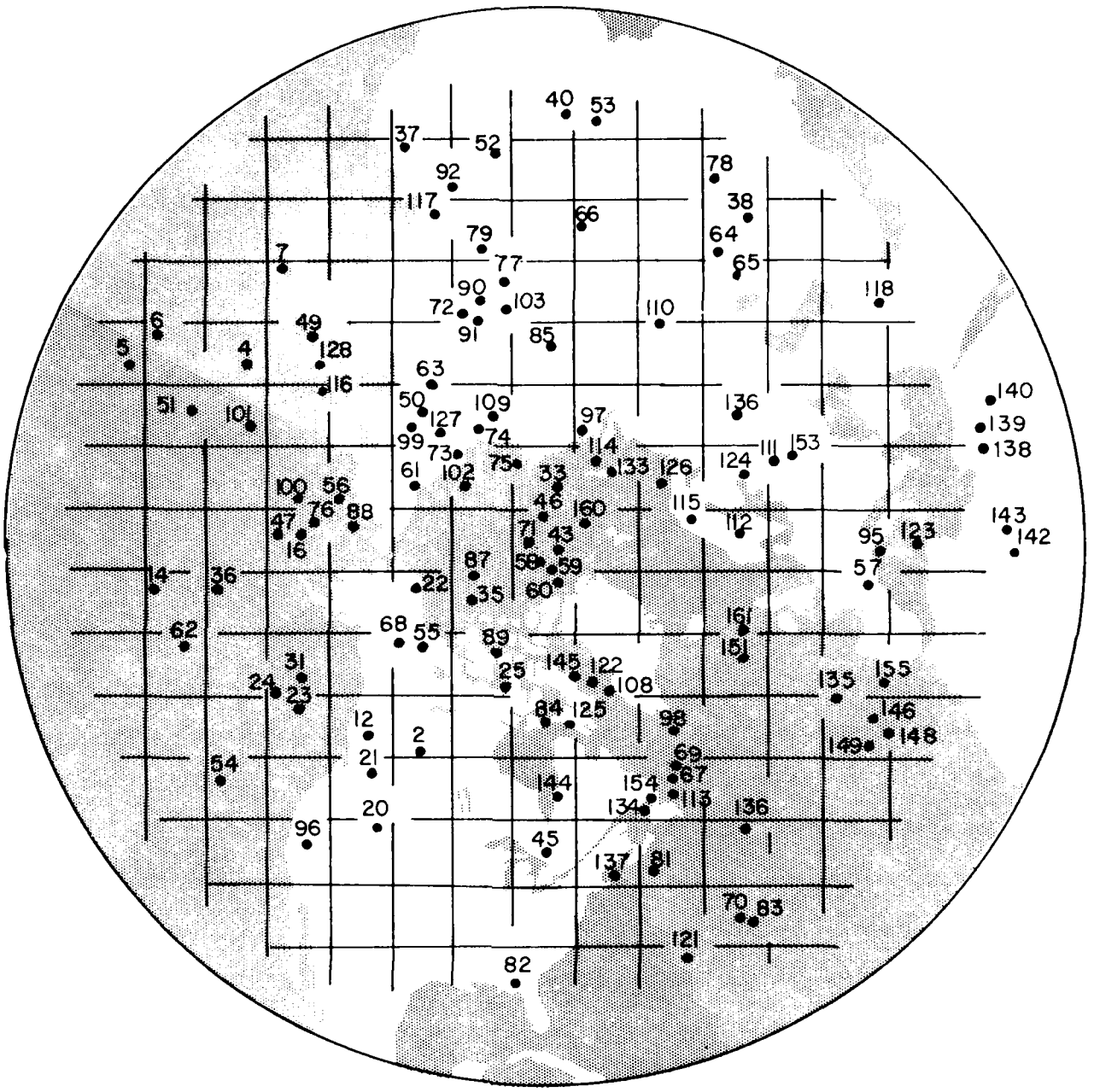

Fig 2b. Nonuniformly distributed final points for trajectories starting at both even and odd numbered gridpoints of Fig 2a and terminating north of $20^{o}N$ latitude.

was made to trace their moving boundaries. Instead, the local mean velocities were used to derive trajectories of the centers of mass as if the bulk systems were completely closed. Obviously, errors are introduced by these approximations. For example, the dispersion along $\pm\nabla\theta$ is really not zero, as assumed, but the dispersion in three-dimensions due to vertical motions is reasonably well approximated.

As mentioned earlier, only half of the trajectories are presented in Fig 1 because the full complement is too difficult to decipher. However, in this reduced set one can see examples of large dispersion, where one bulk parcel moves rapidly away from its initial position, while its' neighbor loops around and then moves off in a different direction. Still others show almost straight line transport where the speed of the bulk parcel equals the local phase speed of the waves.

The net effect is the conversion from an initially uniform distribution, Fig 2a, to an extremely nonuniform distribution, Fig 2b. The initial and final positions are identified by gridpoint numbers, with the trajectories illustrated in Fig 1 being restricted to the odd numbers. In this example, approximately 1/3 of the bulk parcels moved out of the domain to lower latitudes.

The effect of this large-scale transport on the isentropic distribution of potential vorticity is illustrated in Fig 3. The heavy line denotes the threshold value used by Danielsen and Hipskind (1980) to define the dynamic tropopause. Values greater than the threshold have stratospheric properties. In this particular example, the southward extension of the tropopause boundary from Alaska, along the Pacific coast of Canada, and extending across the Rocky Mountains and the Great Plains, was traversed by aircraft equipped to measure radioactivity of stratospheric origin (Danielsen, 1964[1]; 1968). As expected, very large concentrations of strontium 90 and total β activity were

[1]Danielsen, E. F., Report on Project Springfield, DASA 1517, 97 pp., Defense Atomic Support AGency, Washington, D.C., 1964.

Fig 3. Distribution of stratospheric values of potential vorticity on θ= 310k surface, 0000 GMT, 19 April 1963. The heavy line corresponds to the stratospheric threshold of 1.6 x 10^{-5} deg $cm^2(gs)^{-1}$. The analysis is contoured in units of 10^{-7} deg $cm^2(gs)^{-1}$ from 10^2 to 10^3 units. The heavy dashed line corresponds to the spring seasonal mean position of the threshold value, at 60^{o}N latitude.

measured over Wyoming, to the north of the extension.

It is obvious from Fig 3 that the boundary between stratospheric and tropospheric air does not oscillate with small amplitude around the latitude of the zonal mean tropopause. Rather, the amplitudes produced by large-scale wave transports are very large and the pattern in the inclined isentropic surface resembles a breaking wave. The trajectories in Fig 1 are consistent with this deforming pattern and they indicate why it would be extremely difficult to develop a 2-D model based on Lagrangian coordinates.

For example, one could define a Lagrangian average over all longitudinal angles ϕ by the vertical limits $\overline{\theta}_1$ and $\overline{\theta}_2$ and the horizontal limits $\overline{S}_1$ and $\overline{S}_2$ where θ is the potential temperature, S is the potential vorticity and the overbar denotes a local Lagrangian average. The central axis of the zonal average will oscillate north-south with the local mean flow, but when the amplitudes of oscillation become large, dynamic instabilities will generate smaller-scale waves. Then $\overline{S}$ will not be conserved for some of the local bulk parcels and a net transport of potential vorticity out of the zonal Lagrangian system will occur.

Direct evidence for the nonconservation of $\overline{S}$ is obtained from the trajectory analyses. For each of the 160 parcels, $\overline{S}$ was computed every 12 hrs. Approximately 25% of these parcels exhibited fluctuations about a decreasing trend. An examination of these individual trajectories showed that they originated at high latitudes with stratospheric values of potential vorticity, and terminated at lower latitudes with tropospheric values. Direct, in situ measurements of radioactivity confirmed that the decrease in S was associated with a decrease in radioactivity (see Danielsen, 1967[2]).

Since $\overline{S}$ is the mean of some 10^{20} elemental values of S, the non-conservation of $\overline{S}$ does not necessarily imply or even require irreversible processes.

---

[2]Danielsen, E. F., Transport and diffusion of stratospheric radioactivity based on synoptic hemispheric analyses of potential vorticity, USAEC Contr. AT(30-1)-3317, 91 pp., U.S. Atomic Energy Comm., Washington, D.C., 1967.

However, the intermittent transfer of energy to smaller scales tends to proceed toward irreversibility. Thus, the large-scale deformations are the isentropic precursors to small-scale anisentropic processes.

On the basis of these hemispheric trajectory analyses and many other case studies, the author found Lagrangian methods advantageous for understanding the physical processes of transport, but abandoned them for Eulerian methods when attempting to develop an objective method for quantifying the transport in 2-D models. As is evident in Fig 2b, the tendency of Lagrangian parcels to cluster and decluster makes it difficult, if not impossible, to maintain a uniform degree of resolution. Itroducing new parcels intermittently is also self defeating. When a Lagrangian integral is extended to include all longitudes, both the boundaries of the system and the fluxes through the boundaries must be determined. If the system is defined to minimize the flux, the boundary becomes folded and difficult to locate. Conversely, if the system is defined to minimize the deformations of the boundary, the flux becomes large and difficult to quantify.

Nevertheless, the isentropic trajectory and vertical cross-sectional analyses have established that the potential vorticity is a reliable scalar for determining mean and deviatory fluxes and, therefore, a valuable aid to developing a 2-D parameterization for models using either Lagrangian or Eulerian coordinates.

DATA SETS FOR TRANSPORT PARAMETERIZATION

Given the current and rapidly increasing interest in 2-D numerical models for predicting the effects of trace pollutants on atmospheric ozone, the effects of volcanic eruptions on aerosols and their radiative effects on climate, it is obvious that a reliable specification of the mean and deviatory transports is

needed. Assuming that the advantages of Eulerian coordinates will outweigh their disadvantages, one expects Eulerian coordinates to be used in the models. A primary requisite for specifying the transport is a representative set of u,v and w velocity components, and their associated thermodynamic variables at a uniform grid over the globe or at least one hemisphere.

The thermodynamic variables, pressure and temperature, are required for computing the entropy gradients in the potential vorticity. Furthermore, the horizontal gradients, although much smaller than the vertical gradient, cannot be neglected because they are multiplied by the horizontal components of vorticity which are much larger than the vertical components. Thus, a representative data set implies a dynamically balanced, appropriately filtered set that spans the three-dimensional space.

J. Mahlman of the Geophysical Fluid Dynamics Laboratory (GFDL) has developed and tested such a set using the laboratory's General Circulation Model (GCM). The author and S. Hipskind are developing a numerical, diagnostic model to derive another set from the radiosonde observations plus the gridpoint analyses from the National Meteorological Center's numerical prediction model. This work, sponsored by the Federal Aviation Administration, is nearing completion and will be reported separately later. Using both data sets we will first compare the model's velocity statistics to those derived from observations and then compute from each set the gridpoint values for the complete transport tensor.

The rationale developed for this purpose will be described here in considerable detail because it is thought to be generally valid and physically meaningful. However, to set the context, a brief review of previous work will be presented first.

2-D MODEL DEVELOPMENT AND RESULTANT PROBLEMS

Two-dimensional models are based on integrating conservation equations over all longitudes. An additional integration over time, such as a month or a season, is often made but is not essential to this discussion. Thus equations typical of the model take the form

$$\frac{\partial}{\partial t}\left(\bar{\rho}\bar{\chi}_i\right) = -\nabla\cdot\left(\bar{\rho}\bar{V}\bar{\chi}_i\right) - \nabla\cdot\left(\overline{\rho V'\chi_i'}\right) + \bar{S}_i \qquad (1)$$

where ρ, V, χ and S are the density, velocity, mixing ratio and all sources and sinks of species i. Since $\nabla\cdot(\bar{\rho}\bar{V})\simeq 0$ the product $\bar{\rho}\bar{V}$ can be expressed in terms of a stream function $\bar{\psi}$. Also, since χ is a scalar it is customary to use first order closure and express the deviatory flux $\overline{\rho V'\chi'}$ in terms of a scalar product of a diffusion tensor K and the gradient of $\bar{\chi}$ (Stewart, 1945). Thus,

$$-\overline{\rho V'\chi'} = \bar{\rho}\begin{bmatrix} K_{yy} & K_{yz} \\ K_{zy} & K_{zz} \end{bmatrix}\cdot\nabla\bar{\chi} \qquad (2)$$

where the components of the diffusion tensor must be specified as a function of y,z and t.

In one of the first 2-D numerical models, developed by the late B. Davidson, to predict the zonally-seasonally averaged distribution of radioactive aerosols (products of nuclear bomb tests conducted in the atmosphere) the mean circulations were ignored and numerical tests were conducted to determine the appropriate diffusion coefficients. This approach was in marked contrast to the earlier conceptual models of Brewer (1949) to explain the dry stratospheric observations, and of Wolf (1942) and Dobson (1956) to explain the excess ozone at high latitudes. Those conceptual models were focused on mean meridional circulations and, generally, diffusion was neglected.

It was soon discovered that Fickian diffusion, where the off-diagonal

components of K are zero, would not simulate the observed negative slope of the radioactivity isopleths in the stratosphere. It was necessary to introduce negative off-diagonal components and to increase their magnitude until the $\overline{\chi}$ isopleths had a larger negative slope than the potential temperature isotherms $\overline{\theta}$. For details of the model, the resulting simulations and prediction, see Davidson et al., (1966).

The importance of diffusion in transporting radioactive tungsten 185 from the tropical stratosphere was emphasized, also, by Reed and German (1965), although they stressed that, in general, both mean and deviatory transports should be included. They used the mixing length hypothesis, deduced from molecular diffusion or kinetic theory of ideal gases, to express the K's of (2) as products of a mixing length (the Y' or Z' component of a displacement vector) and the appropriate velocity component. Thus, they assumed

$$\chi' = -\mathbf{L}'\cdot\nabla\overline{\chi} = -\frac{\partial\overline{\chi}}{\partial y}Y' - \frac{\partial\overline{\chi}}{\partial z}Z' \tag{3}$$

and showed that

$$\begin{bmatrix} K_{yy} & K_{yz} \\ K_{zy} & K_{zz} \end{bmatrix} = \begin{bmatrix} \overline{v'Y'} & \overline{v'Z'} \\ \overline{w'Y'} & \overline{w'Z'} \end{bmatrix} \tag{4}$$

Then they made the additional assumption

$$\frac{w'}{v'} = \frac{Z'}{Y'} \tag{5}$$

which they considered permissible if the mixing length is small compared with the size of the eddies. As a direct result of this assumption, the off-diagonal components of (4) are equal and therefore the diffusion tensor is symmetric.

To obtain numerical estimates of and to provide a physical explanation of the three remaining terms, K_{yy}, K_{yz} and K_{zz}, they introduced a third assump-

tion

$$\frac{w'}{v'} = \frac{Z'}{Y'} = \tan \alpha \simeq \alpha \tag{6}$$

and expressed (4) as

$$\begin{bmatrix} K_{yy} & K_{yz} \\ K_{yz} & K_{zz} \end{bmatrix} = K_{yy} \begin{bmatrix} 1 & \bar{\alpha} \\ \bar{\alpha} & \bar{\alpha}^2 + \overline{\alpha'^2} \end{bmatrix} \tag{7}$$

where $\bar{\alpha}$ is interpreted as the mean slope of the mixing surface and $\overline{\alpha'^2}$ is the variance of α about $\bar{\alpha}$. For (6) to be valid α must be a small angle. Later we shall see that α is not always small, therefore, assumptions (5) and (6) will be challenged and a more general expression for (4) will be derived.

Numerical values of K_{yy} and $\bar{\alpha}$ were determined from heat flux, temperature, and meridional wind data while $\overline{\alpha'^2}$ was estimated from the vertical rate of spreading of tungsten 185 in tropical latitudes where $\bar{\alpha} \simeq 0$. Reed and German (1965) showed also that, by rotating the coordinates into the principle axis system (which eliminated K_{yz}), the rotation angle $\gamma \simeq \bar{\alpha}$ and the diagonal terms reduce to $K_y = K_{yy}$ and $K_z = \overline{\alpha'^2} K_{yy}$. Since $K_y \gg K_z$, the former correspcnds to the major axis and the latter to the minor axis of the ellipse associated with the matrix (7).

The techniques they introduced were widely accepted and their paper became the standard reference for most 2-D modelers. However, in some of these models, developed after ozone replaced radioactivity as the potential health hazard, little or no attention was paid to the interdependence of the mean and deviatory motions. As shown by Kuo (1956), the mean circulations are forced by horizontal gradients of heating and vertical gradients of frictional forces, both of which are influenced and sometimes dominated by deviatory motions. In particular, thermally indirect circulations, like the Ferrel cell, must be dominated by deviatory motions. Thus, it was obvious to some that mean and

deviatory transports could not be specified independently, and it was also evident, from the structure in tungsten 185 distributions, that both transports were required.

Clearly, balancing these transports in a 2-D model would be challenging. One of the first attempts was made by Louis (1974)[3], who completed a numerical model in which the mean circulations were first derived, and then the coefficients of the diffusion tensor were determined by cancelling the local change in ozone mixing ratio produced by these mean transports. This approach is valid wherever ozone has a chemical lifetime exceeding its' mixing lifetime. Thus, it should be valid below 25 km and invalid about 30 km. In other words, in the upper stratosphere the last term in (1), the source-sink term, can cancel the net effects of the two transports, leaving both of them unconstrained by this approximation.

Two very interesting and perplexing results were obtained from Louis' work. When the model was tested by simulating the transport from equatorial, mid and high latitude nuclear bomb tests, all of the transports were too fast. However, if both the mean and deviatory transports were reduced by 50%, the results were excellent. Since a scalar reduction of both terms would not alter the assumption of a zero ozone tendency, there were two possible explanations. Either the mean circulations were a factor of 2 too fast, or there was a missing scalar coefficient in the transport parameterizations. Although the first explanation was certainly possible it was not highly probable. Furthermore, when Louis' unmodified mean and turbulent transports were used in photochemical models, the poleward transport of ozone was much too slow. Reducing the transports by a factor of 2 to match the radioactivity transport would simply make the ozone transport even slower.

Faced by these conflicting results, modelers understandably adopted a

---

[3] Louis, J. F., A two-dimensional transport model of the atmosphere, Ph.D. Thesis, Dept. of Astrogeophysics, Univ. of Colo., 1974.

pragmatic approach and adjusted the transports to fit their model's predictions of either ozone or radioactive tracers. A comparison of these transport descriptions reveals large differences in the mean velocities and in the diffusion coefficients, not just a factor of 2. In some cases they approach a factor of 20. Why the transports can differ so greatly and still lead to comparable results for a particular trace constituent is another problem that needs explanation. Because the parameterized transports depend on the mean gradients of the species, it is highly improbable that comparable results could be achieved for all species.

In the meantime Mahlman (1975)[4] was taking a different approach. Having completed a tracer experiment in the GCM he could easily generate the mean and deviations of the velocities and tracer mixing ratio. Consequently, he could directly evaluate the two transport terms in (1). His results showed a strong tendency for the two transports to oppose each other, yielding the net transport as a small residual of two large terms. Also, there were locations in the zonal-temporal means where the diffusion flux was not down gradient, thus assumption (2) appeared to be violated. Mahlman also used the two components of the deviatory flux to evaluate the diffusion coefficients. If assumption (2) is made, there are two scalar equations and four unknowns. By adding assumption (3) the unknowns are reduced to three. To reduce them to two, Mahlman assumed

$$\frac{\bar{\rho}\overline{v'\chi'}}{\bar{\rho}\overline{w'\chi'}} = \frac{K_{yy}}{K_{yz}} \tag{8}$$

With this asusmption K_{yy}, K_{yz} and K_{zz} can be determined uniquely as ratios of fluxes and gradients.

---

[4]Mahlman, J. D., Some fundamental limitations of simplified-transport models as implied by results from a three-dimensional general-circulation/tracer model, Proceedings, 4th Conference on the Climatic Impact Assessment Program, DOT-TSC-OST-75-3B, edited by T. M. Hard and A. J. Broderick, U.S. Dept. of Trans., 132-146, 1975.

$$K_{yy} = \frac{\overline{v'\chi'}^{\,2}}{-\overline{\mathbf{V}'\chi'}\cdot\nabla\bar{\chi}} \qquad K_{yz} = \frac{\overline{v'\chi'}\;\overline{w'\chi'}}{-\overline{\mathbf{V}'\chi'}\cdot\nabla\bar{\chi}} \quad \text{and} \quad K_{zz} = \frac{\overline{w'\chi'}^{\,2}}{-\overline{\mathbf{V}'\chi'}\cdot\nabla\bar{\chi}} \qquad (9)$$

Each of these ratios has a common denominator which must be positive if the deviatory flux is down-gradient. As indicated above, negative values were obtained from the GCM results. Although negative values could prove to be troublesome, the fact that the denominator of (9) must pass through zero is even more troublesome. Then at least one of the K's must approach an infinite magnitude.

However, another consequence of assumption (8) is that α'^2 must be negligible compared to $\bar{\alpha}^2$. In other words, the deviatory flux must be effectively limited to an inclined mean stream surface, an assumption used by Fleagle (1955; 1957) to study baroclinic instability. Consistent with Eady's (1949) principle of energy conversions with virtual displacements, Fleagle found that a necessary condition for the amplification of a perturbation in a baroclinic fluid was that the slope δ of the stream surface must be positive but less than the slope δ_θ of the mean isentropes, and that the maximum amplification occurred when $\delta = \frac{1}{2}\delta_\theta$. Conversely, if $\delta > \delta_\theta$ or if the negative slope of the stream surface exceeded the negative slope of the mean isentropes (as indicated above for the stratosphere) the perturbations were damped.

This concept was used by Newell (1961) to explain the counter-gradient heat flux in the stratosphere, by Reed and German (1965), and by Louis (1974)[3] to parameterize the diffusion coefficients in the troposphere and stratosphere. It also figures prominently in the work of Green (1970). In the troposphere, where kinetic energy must be generated to account for both energy flux into the stratosphere and dissipation of energy at the earth's surface, δ must

[3] Ibid.

approach $\frac{1}{2}\delta_\theta$, i.e., the implied correlation between ascending motion and warm advection, descending motion and cold advection, must reduce the local change by advection. Indeed, at 500 mb the observed local change in temperature is about one-half of the observed advective change. Thus, there is observational and theoretical evidence to support Mahlman's assumption (8) which implies that the wave motions are linearly polarized, but Fleagle's (1957) results indicate that the unstable waves will become elliptically polarized and therefore $\overline{\alpha'^2}$ will grow. Again, we are confronted by an apparent inconsistency that remains to be resolved.

Last, but not least, a new challenge to the use of a diffusion tensor for elliptically polarized wave-particle velocities was raised by Wallace (1978). He asserts that the stream surfaces in the lower stratosphere will have positive slopes, not the negative slopes assumed by the previously discussed authors, and attributes the meridional counter-gradient fluxes to Stokes drift[1]. Large-scale waves in the lower stratosphere are assumed by Wallace to be evanescent; amplitudes decreasing with height and with distance north and south of an axis of maximum amplitude. He then deduces from the kinematics of the elliptically polarized velocity distributions a mean particle drift downward to the north of the axis and one upward to the south of the axis. The combined, torque-like action of these two drifts is claimed to be responsible for the counter-gradient fluxes. However, these drifts are apparently isentropic since Wallace explicitly neglects diabatic cooling and makes no mention of irreversible small-scale mixing.

---

[1]Stokes drift is a mean particle drift or streaming velocity produced in a homogeneous fluid, i.e., in the absence of a restoring force, by amplitude gradients of elliptically polarized isentropic wave motions.

MEAN CIRCULATIONS: STREAMLINES OR TRAJECTORIES

When large-scale, quasi-horizontal wave motions in the atmosphere have a definite axis of maximum amplitude, it will generally correspond to the axis of a jet stream. Now, it is well known that when velocities are averaged longitudinally and temporally (not at constant latitude but at a constant distance from the axis of a jet) the resulting mean circulations are direct like the Hadley, not indirect like the Ferrel cell circulations. After Fultz and Riehl (1957) determined a direct circulation from their annular dishpan experiments, Krishnamurti (1961) showed that the subtropical jet had a similar circulation. Later, Mahlman (1973) found that averaging relative to the polar jet also yielded similar results.

These jet rectified circulations in the northern hemisphere include ascending motions along the entropy gradient on the anticyclonic (south) side of the jet, northward flow along the potential vorticity gradient above the jet core, then descending motion against the entropy gradient on the cyclonic side, and jet core. Although the upward and downward branches are similar in sense and location to the mean drifts deduced by Wallace (1978), they cannot be attributed to isentropic processes.

In addition to having different characteristic values of potential vorticity, the upward and downward branches have different concentrations of trace constituents. As shown by Danielsen et al., (1962)[5], radioactive isotopes measured from aircraft during the spring of 1960 were predominantly of stratospheric (tropospheric) origin when measured on the cyclonic (anticyclonic) side of both the polar and subtropical jets. In particular, strontium 89 and barium 140, produced in the troposphere by a specific bomb test, were present in large concentrations on the anticyclonic sides but were either absent or

[5]Danielsen, E. F., K. Bergman and C. Paulson, Radioisotopic potential temperature and potential vorticity - a study of stratospheric-tropospheric exchange processes, Dept. of Meteorology and Climatology, Univ. of Washington, 54 pp., 1962.

below detectable limits on the cyclonic sides.

These data suggest that such jet rectified mean circulations are not closed Lagrangian circulations, i.e., they do not represent the trajectories of air parcels, even bulk, semiclosed air parcels. An air parcel crossing above the axis of the jet must change its potential vorticity and trace constituents too rapidly to be compatible with small-scale mixing with the parcel's environment. On the other hand, there is ample evidence that the descending branch of the circulation is Lagrangian or quasi-Lagrangian.

One example comes from the same, above mentioned aircraft experiment. When the measured concentrations of strontium 90, tungsten 185, and berylium 7 were plotted versus θ as the ordinate and S as the abscissa, the strongest concentrations of each isotope were almost independent of θ over the entire observational range, 325 to 390°K and 10 to 15 km in height. Although all three isotopes are considered as stratospheric tracers, we know most explicitly the initial conditions for tungsten 185. It was introduced as a tracer in the tropical Hardtack series (summer of 1958) and aircraft and balloon measurements showed that its maximum concentrations were from 380 to 480°K in θ and from 16 to 20 km in height.

Obviously, the tungsten moved downward in elevation as it moved northward from the tropical latitudes, but it is equally obvious that it did not descend isentropically. Like the descending branch of the jet rectified mean circulation, the tungsten crossed the θ surfaces towards decreasing values, equivalent to a net cooling of 60 to 80°K in potential temperature, on the cyclonic (north) side of the major jets. Therefore, the radioactivity data indicate that the descending branch of the jet rectified circulation represents a material drift, but it cannot be attributed to Stokes drift.

When air parcels move isentropically along elliptical paths, their vertical

displacements are limited to those of the entropy surfaces themselves. Therefore, when mean circulations cross mean entropy surfaces but the parcel motions are isentropic, the mean flow lines are streamlines connecting the velocities of different air parcels (each having a different entropy) and no individual parcel follows the streamlines, even under steady state conditions. Thus, the entropy gradient precludes a material cross-entropy drift developing from purely isentropic motions.

The downward transport of the stratospheric tracers requires an additional diabatic cooling gradient and/or small-scale, irreversible mixing. When diabatic cooling increases with latitude the isopleths of the trace species will rotate relative to the mean isentropes in the required sense. However, to maintain the observed positive correlation between the trace species and the potential vorticity, $\frac{\partial}{\partial\theta}\left(\frac{d\theta}{dt}\right)$ must be much smaller than the meridional gradient at constant θ. In particular, these conditions are deemed necessary to explain the large deviations between $\overline{S}^{L}$, the synoptic or local mean, and $\overline{S}^{Z}$, the zonal-seasonal mean of potential vorticity shown in Fig 4. For the synoptic cross-section of potential temperature and wind speed, plus the correlation with ozone, see Danielsen (1968).

At high latitudes $\overline{S}^{L}$ oscillates about $\overline{S}^{Z}$ so closely that only one set of isopleths is labelled. However, above and to the north of the almost merged polar and subtropical jets, $\overline{S}^{L}$ oscillations are very large and, consequently, the deviations $\overline{S}^{L} - \overline{S}^{Z}$ are also large. Between Tallahassee (station 72214) and Bedford (station 72490) the $\overline{S}^{L} = 800$ isopleth drops 10 km in elevation and decreases 150^{o}K in Θ (from 476 to 325^{o}K).

Those large deviations in height and Θ greatly exceed the height and θ range of the $\overline{S}^{Z} = 800$ isopleth from 20^{o}N to the pole. Therefore, they cannot be explained by horizontal displacements of the zonal mean values. In parti-

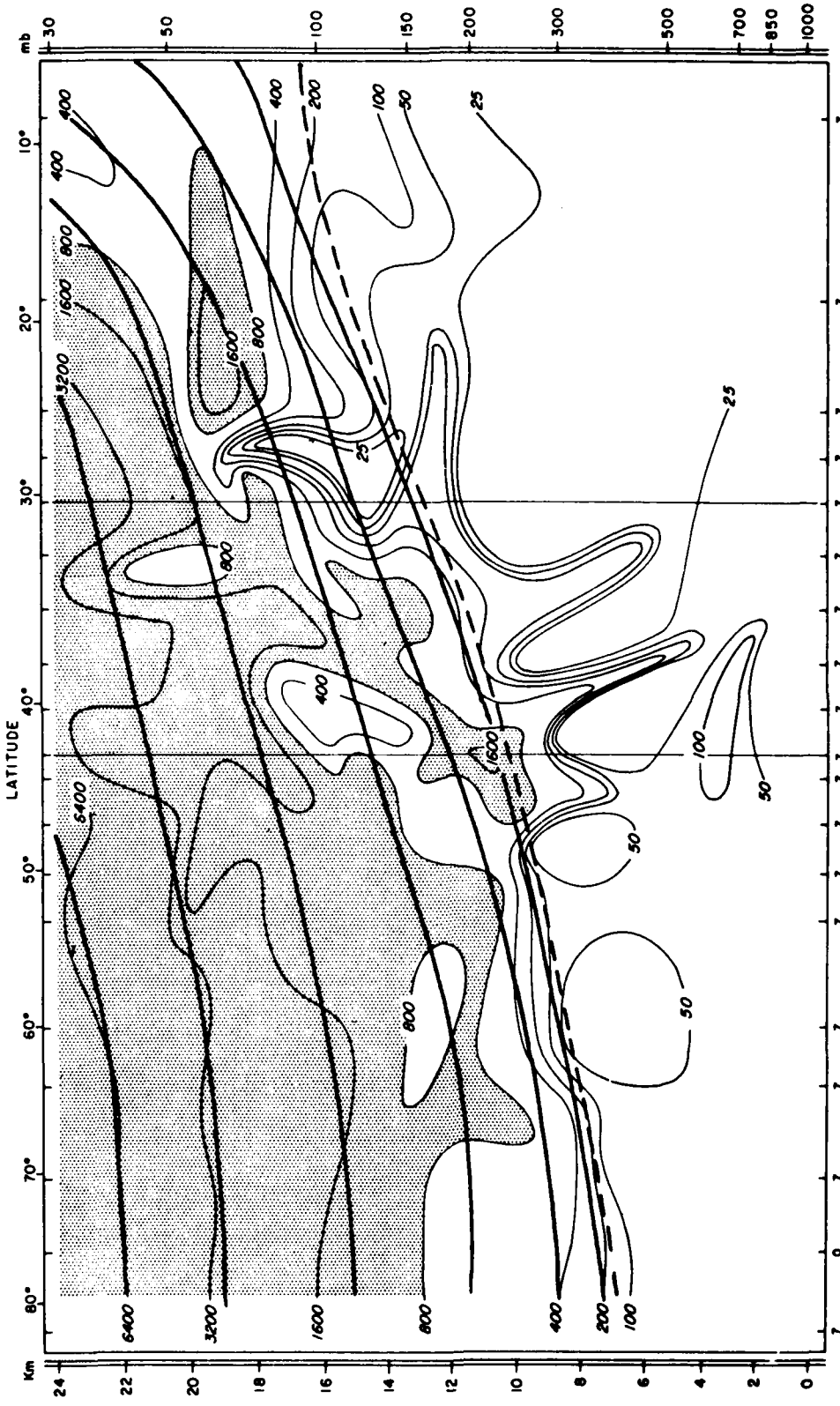

Fig 4. Vertical cross section of potential vorticity from 80 to 10°N along the 80th meridian west of Greenwich. The light contours in units of 10^{-7} deg $cm^2(gs)^{-1}$ are the synoptic values of potential vorticity; the heavy controus are the corresponding spring seasonal-longitudinal mean values. The two vertical lines denote the location of special ozone soundings at tallahassee, Fla. (72214) and Bedford, Mass. (72490).

cular the $\bar{S}$ = 1600 maximum at 10 km over Bedford is more than 5 km below the minimum elevation of the zonal mean and approximately 75° colder than the minimum θ of the zonal mean. Furthermore, this 1600 maximum could not have been generated locally by a vertical gradient of $\frac{d\theta}{dt}$ because the ozone deviations correlate with the potential vorticity deviations. The physical explanation offered by Danielsen et al., (1962)[5] and the schematic diagram of the circulations (Fig 16 of the same reference) still appear to be valid. They attributed the decreasing entropy transport primarily to radiative cooling over the cold cirrus cloud shields, above and to the north of the jet axis, and depicted the ascending and descending branches as separate Lagrangian flows which mix actively in certain regions, but which do not form a closed Lagrangian circulation.

Although an isentropic Stokes drift might represent the difference between the constant latitude mean circulations and the jet rectified mean circulations, it does not appear to be responsible for the negative slopes of the mean or synoptic isopleths of stratospheric trace species concentrations.

ANALYSES OF THE DEVIATORY VELOCITY TENSOR

To test this conclusions, gridpoint values of the velocities for one January realization of the GFDL's general circulations model were analyzed. Granted, one realization is not sufficient, but it was thought to be necessary and it provided a basis for program development and for future comparisons with objectively derived velocities from synoptic data. At four pressure levels - 38, 65, 110 and 190 mb - and three latitudes - 24, 48 and 72°N - the u,v and w gridpoint values were averaged and subtracted from the grid values to determine the deviations. Then the following terms in the deviatory velocity tensor were computed.

---

[5] Ibid.

$$\begin{bmatrix} \overline{v'v'} & \overline{v'w'} \\ \overline{w'v'} & \overline{w'w'} \end{bmatrix} = \overline{v'v'} \begin{bmatrix} 1 & \gamma \\ \gamma & \gamma^2+\beta^2 \end{bmatrix} = \frac{V_o V_o}{2} \begin{bmatrix} 1 & \frac{W_o}{V_o}\cos\phi_o \\ \frac{W_o}{V_o}\cos\phi_o & \left(\frac{W_o}{V_o}\right)^2 \end{bmatrix} \tag{10}$$

In the central matrix array, $\gamma = \frac{\overline{v'w'}}{\overline{v'v'}}$ represents the angle between the principle axis of the associated ellipse and the v or y axis, and β^2 is the ratio of its minor to major axis. Note that the determinant of the central array is equal to β^2, and in the principle axis system the off-diagonal elements are zero and the diagonal elements are 1 and β^2.

The matrix array on the right has special significance, especially for computing and interpreting the deviatory velocity tensor. We can think of the associated ellipse as being generated by a single wave whose components are

$$v = V_o \cos\phi \tag{11a}$$

$$w = W_o \cos(\phi + \phi_o) \tag{11b}$$

where ϕ denotes the longitudinal angle and ϕ_o is a relative phase angle. By forming the appropriate products from (11a) and (11b), and integrating over all longitudes, it is readily shown that the matrix array on the right of (10) is generated.

The significance of this equivalent monochromatic wave is revealed by expanding v' and w' in a Fourier series, forming their products and integrating over all longitudes. Since only a relative phase angle is important, let

$$v'(\phi) = \sum_{m=1} V(m)\cos m\phi \tag{12a}$$

$$w'(\phi) = \sum_{\mu=1} W(\mu)\cos(\mu\phi + \phi_\mu) \tag{12b}$$

then, for example

$$\overline{v'w'} = \sum_m \frac{V(m)W(m)}{2} \cos\phi_m = \frac{V_o W_o}{2} \cos\phi_o \qquad (13)$$

and all terms with $\mu \neq m$ vanish. Therefore, $\bar{\rho}\overline{v'v'}$ can be represented by $\frac{\bar{\rho} V_o V_o}{2}$ which is the kinetic energy density of the meridional deviatory motions. Also, since $V_o \gg W_o$, we can consider it the kinetic energy density of the deviatory motions.

It is clear from (13) and (10) that the deviatory velocity tensor can be written as the sum of the wave number tensors. Also, the equivalent ellipse can be expressed as the sum of the individual ellipses associated with each wave number. This result is very convenient because it is easy to evaluate the Fourier coefficients and the relative phase angles. The relative phase between v'(m) and w'(m) determines the properties of the ellipse. From the equality of the determinants of the central and right matrix arrays (10), it can be shown that

$$\beta^2 = \left(\frac{W_o}{V_o}\right)^2 \sin^2\phi_o \qquad (14)$$

therefore, if $\phi_o = 0, \pi$ the minor axis of the ellipse vanishes and the velocities are linearly polarized. Furthermore, since $\cos\phi_o$ then equals 1, the right matrix depends only on v_o and w_o. Thus, $\phi_o = 0, \pi$ is equivalent to Mahlman's assumption (8), and $\gamma = \frac{W_o}{V_o}$. In this case, Reed and German's interpretation of $\bar{\alpha}$ as the mean slope of the mixing surface is unambiguous.

However, when $\beta^2 \neq 0$ the velocities v_o and w_o are elliptically polarized. This mean that at some longitude, w' will be finite when v' = 0, thus violating Reed and German's assumption that α is a small angle. On the other

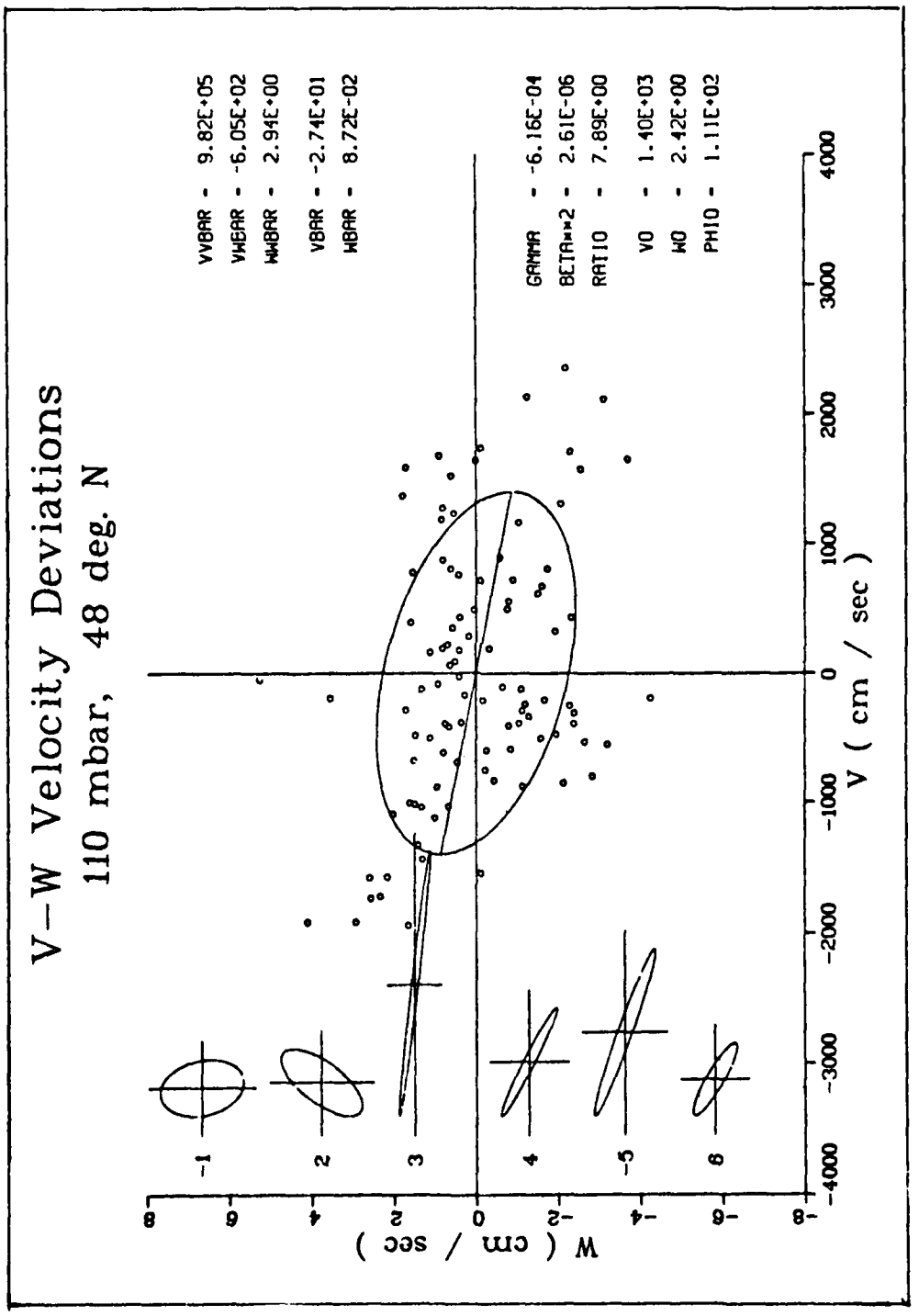

Fig 5a. Meridional-vertical velocity correlations from the Geophysical Fluid Dynamics Laboratory's General Circulation Model. The gridpoint values are the small, open circles which scatter about the equivalent ellipse and the line denoting the slope of its principle axis. Individual wave number ellipses are plotted at the left with a minus sign indicating anticyclonic or clockwise rotation versus increasing east longitude, at gridpoint 110 mb, 48 deg. N.

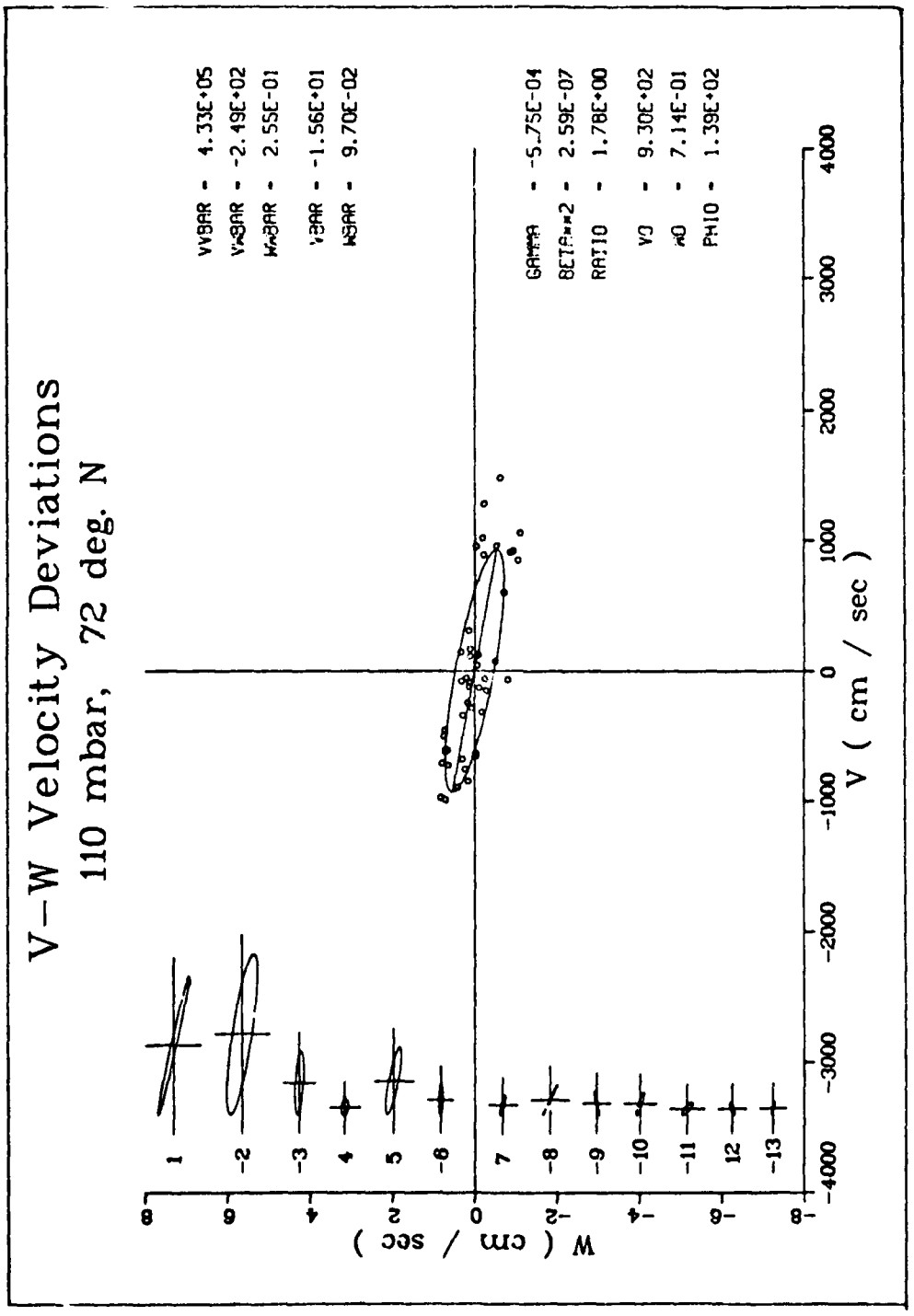

Fig 5b. Same as Fig 5a, except at gridpoint 110 mb, 72 deg. N.

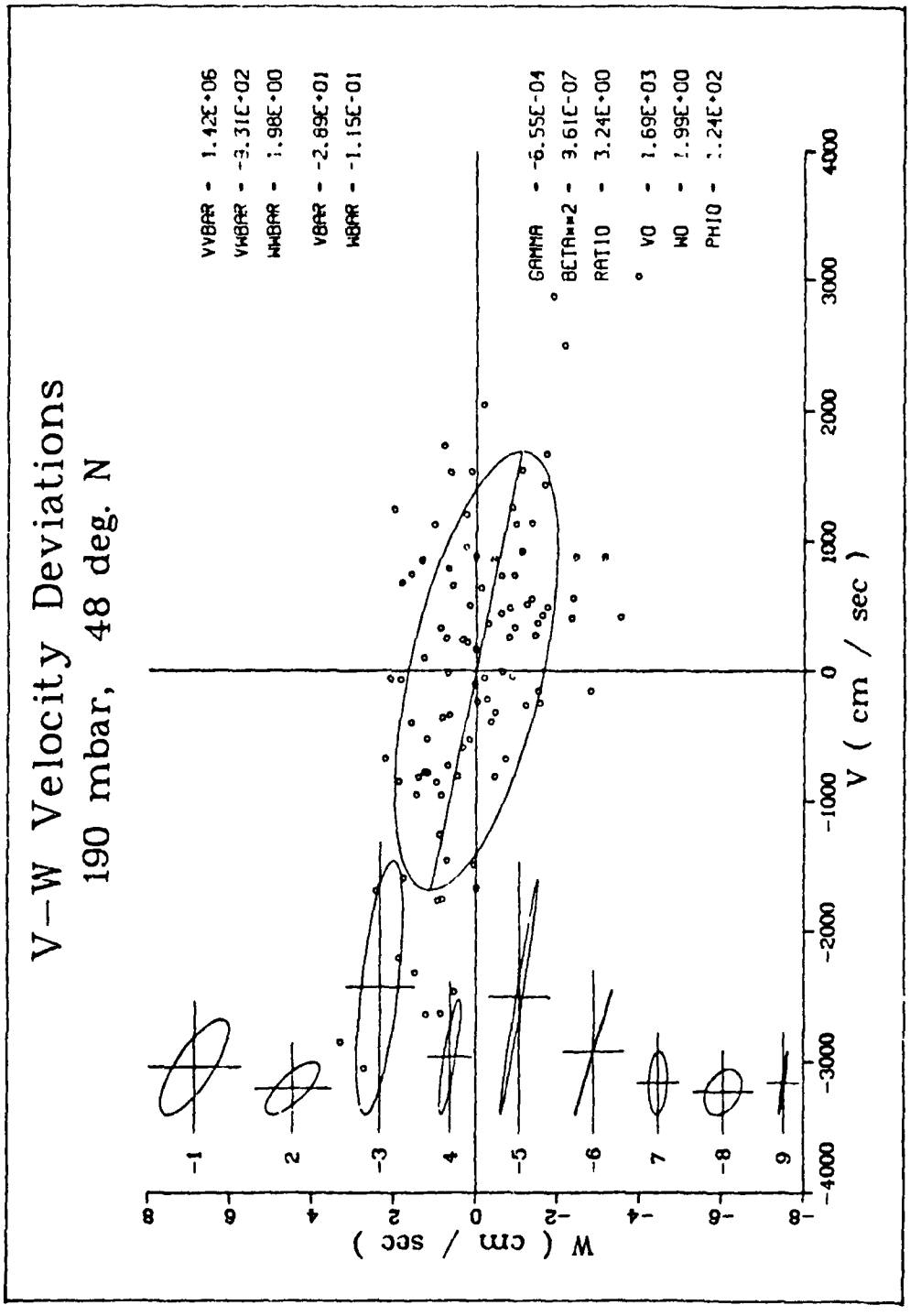

Fig 5c. Same as Fig 5a, except at gridpoint 190 mb, 48 deg. N.

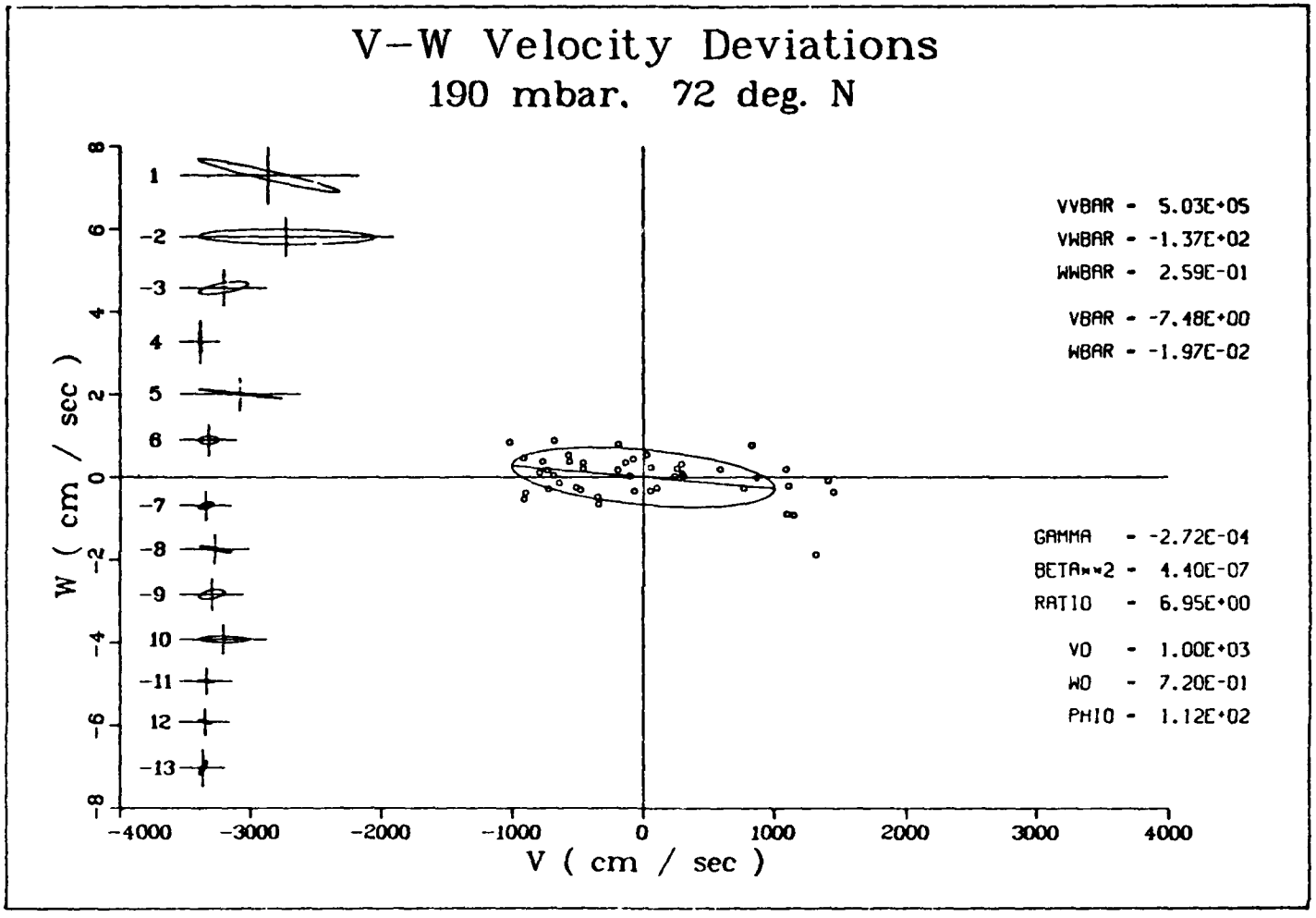

Fig 5d. Same as Fig 5a, except at gridpoint 190 mb, 72 deg. N.

hand, γ is a small angle and it, not $\overline{\alpha}$, defines the mean slope of the mixing surface. Therefore, γ, the principle angle of the ellipse, is the relevant angle for the general case.

Four examples of the individual wave number ellipses and the total ellipse are presented in Fig 5, along with the gridpoint values from which they were derived. In each example, the v', w' points scatter about an ellipse whose major axis slopes downward towards the pole. Also, it can be shown that these slopes exceed the mean slope of the θ surfaces at the same gridpoints, thus a counter-gradient heat flux is implied.

This evidence does not support Wallace's assertion that the ellipses will have a positive slope in the lower cyclonic stratosphere, nor does it support Mahlman's implicit assumption of linear polarization. Conversely, it does support Newell's interpretation and the inclusion of $\overline{\alpha'^2}$ by Reed and German, and by Louis. Note, however, that $\overline{\alpha'^2}$ must be interpreted via β^2 as describing the departure from linear polarity. That such departures can be large can be seen in Fig 6, which illustrates the ellipses at 65 and 190 mb and 24°N. Both ellipses have small positive γ's and are quasi-circular in these plots. Of course, the w' scale is distorted by about 400 to 1, but this is a realistic distortion for the atmospheric asymmetries. The positive slope at 190 mb is expected because it is in the mean troposphere, south of the extra-tropical jet. The slope at 65 mb is too small to be significant, meaning that $\overline{v'w'}$ is small because $\phi_o \simeq \pi/2$. In this case it is 87°.

Figures 5 and 6 clearly demonstrate the prevalence of elliptical polarity between v' and w'. But they indicate, also, that the component wave number ellipses can differ significantly from each other. In general, when $\gamma(m)$'s include both positive and negative values, the scatter of the v', w' points about the equivalent ellipse is large and it has small eccentricity.

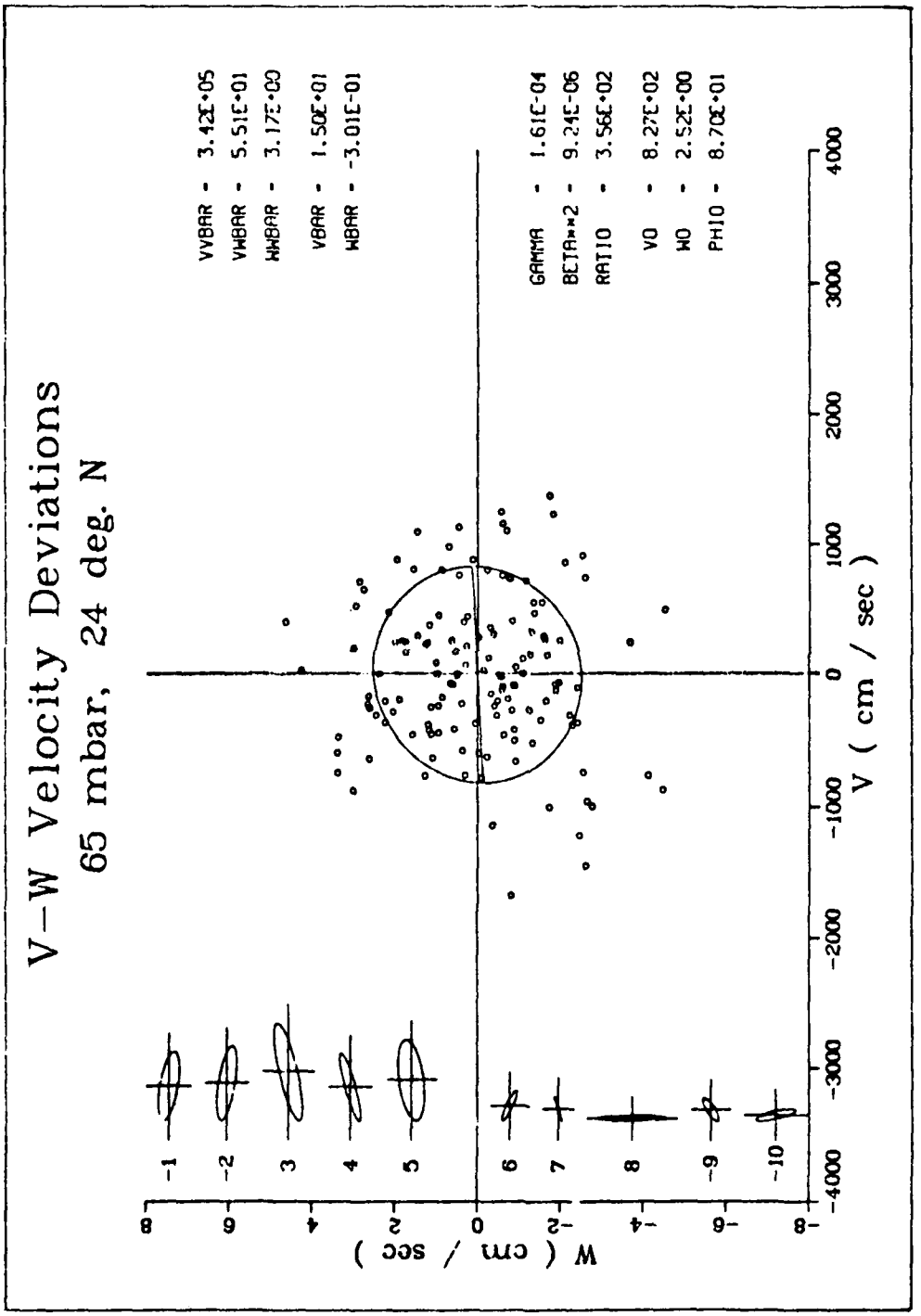

Fig 6a. Same as Fig 5a, except at gridpoint 65 mb, 24 deg. N.

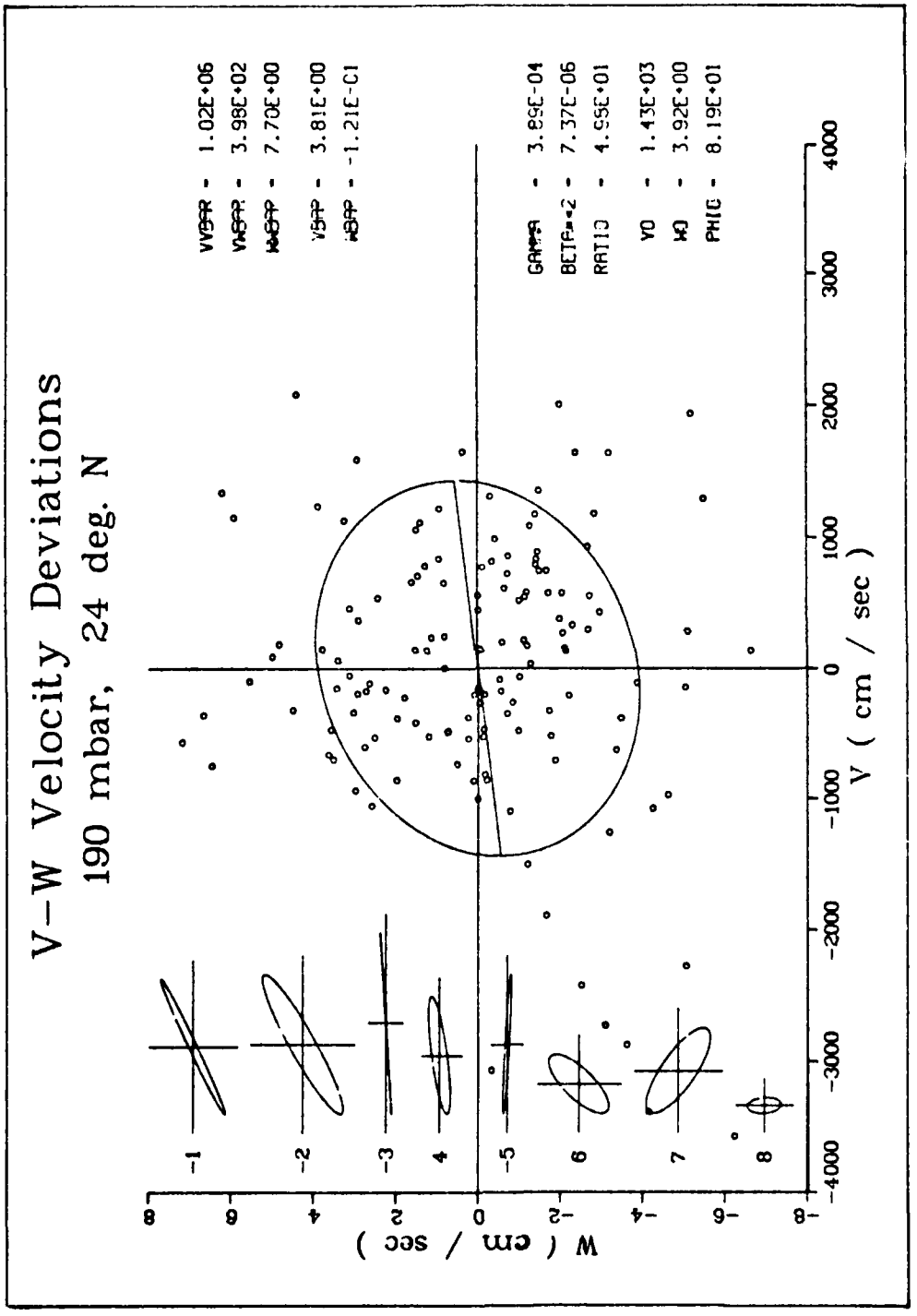

Fig 6b. Same as Fig 5a, except at gridpoint 190 mb, 24 deg. N.

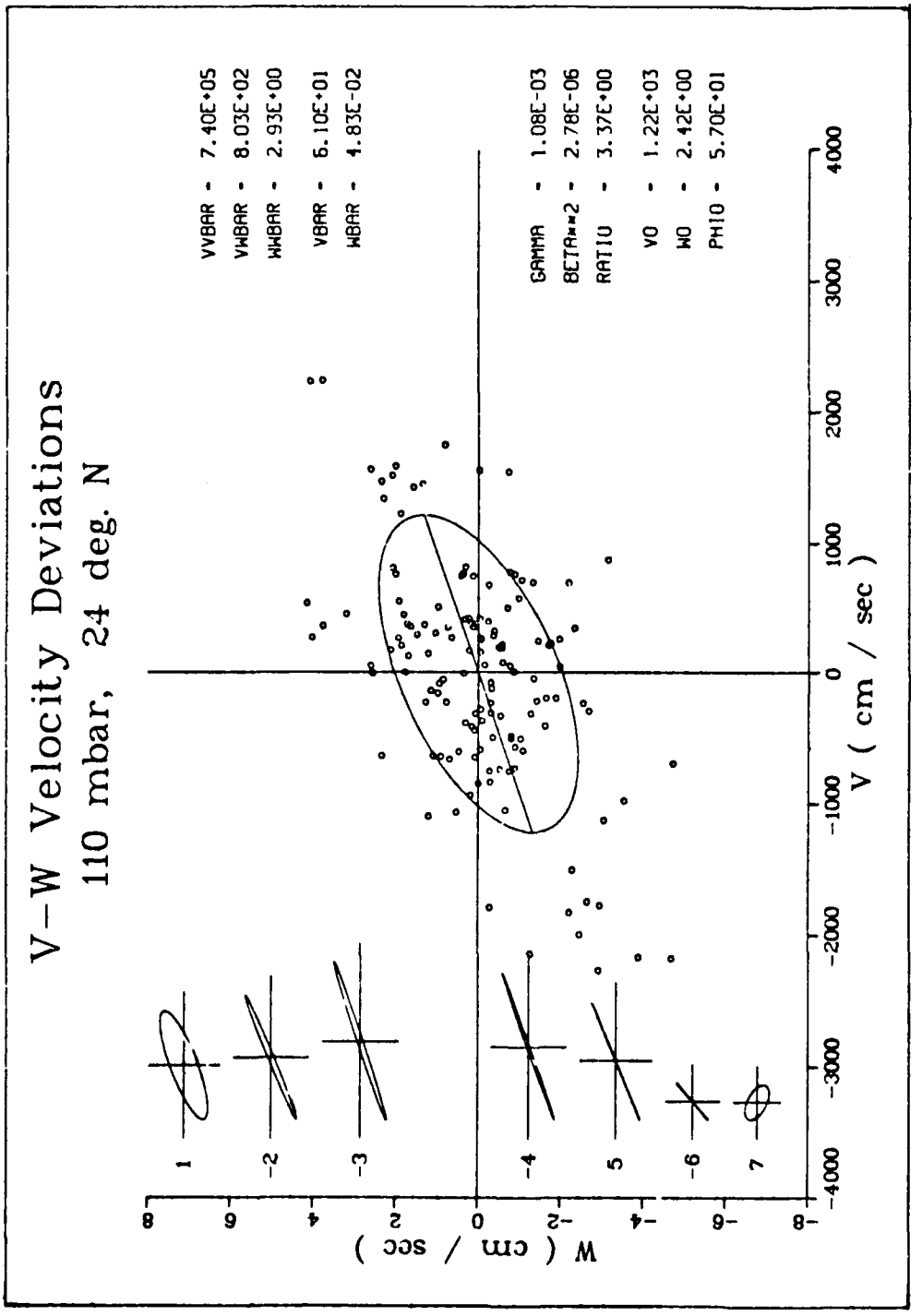

Fig 7. Same as Fig 5a, except at gridpoint 110 mb, 24 deg. N.

There is evidence, also, of linear polarity for some wave numbers. In this respect, the plot for Fig 7, 100 mb and 24°N, is particularly interesting. Wave numbers 2 through 5 are all linearly polarized and all have positive slopes. This gridpoint is located in the lower, anticyclonic stratosphere where the $\bar{\theta}$ isotherms have a small negative slope. Therefore, the linear polarity and positive slopes for γ imply the local change in θ exceeds that due to advection, and warm (cold) advection is correlated with descending (ascending) motions. It remains to be seen whether this result is an artifact of the model or if the atmospheric diagnostic analyses will confirm it. If it is confirmed, it has important implications for tropospheric-stratospheric exchange at subtropical latitudes.

PHYSICAL SIGNIFICANCE OF AN ASYMMETRIC TENSOR

In a review article on stratospheric transport, Danielsen and Louis (197 showed that transport by mean circulations could be incorporated into the diffusion tensor, but that the generalized tensor would no longer be symmetric. This result follows from the condition mentioned earlier, that $\nabla\cdot(\bar{\rho}\bar{\mathbf{V}}) \simeq 0$ and, therefore

$$\bar{\rho}\bar{\mathbf{V}} = \nabla \times (\bar{\psi}\,\mathbf{i}) \tag{15}$$

where $\bar{\psi}$ is a stream function for the mean momentum density and $\mathbf{i}$ is a unit vector in the zonal direction. Then, by use of vector identities, one can write

$$\nabla\cdot(\bar{\rho}\bar{\mathbf{V}}\bar{\chi}) = \nabla\cdot\begin{bmatrix} 0 & \bar{\psi} \\ -\bar{\psi} & 0 \end{bmatrix}\cdot\nabla\bar{\chi} \tag{16}$$

When this antisymmetric tensor is added to the diffusion tensor, the entire

transport is specified by a single asymmetric tensor

$$-\nabla\cdot\left(\bar{\rho}\bar{V}\bar{\chi}+\bar{\rho}\overline{V'\chi'}\right)=\nabla\cdot\bar{\rho}\begin{bmatrix}K_{yy} & K_{yz}+\frac{\Psi}{\bar{\rho}}\\ K_{zy}-\frac{\Psi}{\bar{\rho}} & K_{zz}\end{bmatrix}\cdot\nabla\bar{\chi} \tag{17}$$

The next and crucial question is whether $K_{zy} = K_{yz}$. If they are not equal, their mean value will contribute to a symmetric tensor and their differences will contribute to the antisymmetric tensor. In other words, if they are not equal, the mean flow will be modified, since it is represented by the antisymmetric tensor.

Sommerfeld (1950), in discussing antisymmetric tensors, stresses that they can be represented by axial vectors. The curl operator (15) generates an axial vector, thus, the stream function and the vorticity associated with it should appear explicitly and implicitly, respectively, in the antisymmetric part of the tensor. Indeed, the mean circulations do represent vorticity in the zonal direction since

$$\nabla\times\left(\bar{\rho}\bar{V}\right)=-\nabla^2\bar{\Psi} \tag{18}$$

The mean flow expressed in terms of $\bar{\Psi}$ in (17) is the Eulerian mean, part of which is derived by diabatic, irreversible processes and part by isentropic processes. If the latter are significant, the stream function associated with them must be subtracted from the former and, therefore, $K_{zy} \neq K_{yz}$.

In a recent work by Matsuno (1980), this conclusion follows as a necessary condition for consistency with his assumption. That is, he analyzes the highly simplified case of a single, vertically propagating planetary wave (no. 1), which is locally stationary in a barotropic, channel-type mean flow. But, this simplicity permits him to obtain analytical solutions to the transport

which are very revealing. In this author's opinion, they provide the key to the resolution of most (perhaps even all) of the above noted problems.

The key is Matsuno's (1980) generalization of the mixing length hypothesis. By introducing a mixing time τ defined by

$$\tau \equiv \frac{\overline{\chi} - \chi}{d\chi/dt} \tag{19}$$

assumption (3) is replaced by an integral

$$\chi'(0) = \int_{T \to -\infty}^{0} \frac{e^{t/\tau}}{\tau} \left(\frac{\partial \overline{\chi}}{\partial y} Y' + \frac{\partial \overline{\chi}}{\partial Z} Z' \right) dt \tag{20}$$

where Y' and Z' are now functions of time.

In particular, if they are harmonic functions of time, oscillating with a single, circular frequency ω and describing elliptical paths, as they are in his idealized example, the flux vector he derives is

$$-\overline{\mathbf{v}'\chi'} = \left[\Phi_1 \mathbb{K}'_S + \Phi_2 \mathbb{K}'_A \right] \cdot \nabla \overline{\chi} \tag{21}$$

where $\mathbb{K}'_S$ denotes a symmetric tensor, similar in form to that of Reed and German (1965) except that it describes the effects of wave number 1 only, and $\mathbb{K}'_A$ denotes an antisymmetric tensor whose divergence acts to oppose the mean flow. The most revealing parts of this result are the scalar weighting factors.

$$\Phi_1 = \frac{\omega\tau}{1+\omega^2\tau^2} \qquad \Phi_2 = \frac{\omega^2\tau^2}{1+\omega^2\tau^2} \tag{22}$$

To be rigorously consistent with his model assumptions, which include no mixing processes and no diabatic heating, τ must be infinitely large. Then Φ_1

vanishes, $\Phi_2 = 1$ and the trivial solution $\frac{\partial \bar{\chi}}{\partial t} = 0$ is achieved. The vanishing of Φ_1 is consistent with no mixing processes and when $\Phi_2 = 1$ the negative of the Stokes drift cancels the mean circulation. It should, for in the absence of frictional forces and diabatic heating, the only contribution of the mean circulation is that due to Stokes drift.

On the other hand, if τ is finite due to chemical-photochemical reactions, then there will be a net transport which must be counteracted by the source-sink term in (1) to maintain steady state. By relaxing his initial assumptions, Matsuno estimated $\tau \simeq 10^7$ sec, attributing it to smaller-scale mixing and/or chemical processes. Under these circumstances, $\Phi_1 \simeq 10^{-2}$ and $\Phi_2 \simeq 1$. Therefore, he concludes that, "the eddy transport is advective rather than diffusive in nature and, in effect, it represents transports due to Stokes drift."

We will return to this conclusion later because these are reasons for rejecting his value of τ as being much too large. Therefore, although we can disagree with his conclusions, we can profit by his generalizations of the diffusion approximation.

METHOD FOR DETERMINING ASYMMETRIC DIFFUSION TENSOR

Given a set of u,v and w velocities, the zonal means $\bar{u}, \bar{v}$ and $\bar{w}$ can be readily computed and, from the meridional-height distribution of $\bar{\rho}\bar{v}$ and $\bar{\rho}\bar{w}$ a stream function can be derived. Then, from $\overline{u'v'}$, $\overline{v'w'}$ and $\overline{w'w'}$, as shown in (9) and (19), the equivalent velocities v_o and w_o, plus the relative phase angle ϕ_o can be evaluated. Associated with these velocities will be some, as yet unknown, equivalent ω_o. Therefore, if we generalize (11) as

$$V' = V_0 \cos(\omega_0 t + \phi_1) \quad , \qquad W' = W_0 \cos(\omega_0 t + \phi_2) \tag{23}$$

the associated displacements from the origin are

$$Y' = \frac{V_o}{\omega_o}\left[\sin(\omega_o t + \phi_1) - \sin\phi_1\right], \quad Z' = \frac{W_o}{\omega_o}\left[\sin(\omega_o t + \phi_2) - \sin\phi_2\right] \tag{24}$$

where

$$\phi_2 = \phi_1 + \phi_o \tag{25}$$

If (24) are substituted into (20) and integrated

$$\chi'(o) = \frac{-V_o}{\omega_o}\frac{\partial\bar{\chi}}{\partial y}\left[\Phi_1\cos\phi_1 + \Phi_2\sin\phi_1\right] - \frac{W_o}{\omega_o}\frac{\partial\bar{\chi}}{\partial z}\left[\Phi_1\cos\phi_2 + \Phi_2\sin\phi_2\right] \tag{26}$$

Next, multiplying (26) by (23), after setting t = 0, and then integrating over all longitudes (here ϕ_1 and ϕ_2 are functions of longitude) one obtains

$$-\bar{\rho}\overline{V'\chi'} = \left\{\bar{\rho}\begin{bmatrix}\frac{V_oV_o}{2} & \frac{V_oW_o}{2}\cos\phi_o \\ \frac{V_oW_o}{2}\cos\phi_o & \frac{W_oW_o}{2}\end{bmatrix}\frac{\Phi_1}{\omega_o} + \begin{bmatrix}0 & \bar{\rho}\frac{V_oW_o}{2}\sin\phi_o \\ -\bar{\rho}\frac{V_oW_o}{2}\sin\phi_o & 0\end{bmatrix}\frac{\Phi_2}{\omega_o}\right\}\cdot\nabla\bar{\chi} \tag{27}$$

In (27) all terms involving $\bar{\rho}, V_o, W_o$ and ϕ_o can be determined from the representative data set, as can $\bar{\rho}\overline{V'\chi'}$ and $\nabla\bar{\chi}$. Thus, (27) includes two scalar flux equations and contains two unknowns, $\frac{\Phi_1}{\omega_o}$ and $\frac{\Phi_2}{\omega_o}$. Both unknowns have dimensions of time and we can denote the first by T_1. However, it will be convenient to factor out the common term in the antisymmetric tensor and set the second unknown as a stream function for the oscillatory motions, i.e,

$$\psi_o = \frac{\Phi_2}{\omega_o}\bar{\rho}\frac{V_oW_o}{2}\sin\phi_o \tag{28}$$

With this notation (27) becomes

$$-\rho\overline{\mathbf{V}'\chi'}=\left\{\rho\begin{bmatrix}\frac{V_oV_o}{2} & \frac{V_oW_o}{2}\cos\phi_o\\ \frac{V_oW_o}{2}\cos\phi_o & \frac{W_oW_o}{2}\end{bmatrix}T_1+\begin{bmatrix}0 & 1\\ -1 & 0\end{bmatrix}\psi_o\right\}\cdot\nabla\bar{\chi} \tag{29}$$

where T_1 and ψ_o are now the two unknowns.

The solutions are

$$T_1=\frac{-\bar{\rho}\overline{v'\chi'}\frac{\partial\bar{\chi}}{\partial y}-\bar{\rho}\overline{w'\chi'}\frac{\partial\bar{\chi}}{\partial z}}{\rho\left(\frac{V_oV_o}{2}\frac{\partial\bar{\chi}}{\partial y}^2+V_oW_o\cos\phi_o\frac{\partial\bar{\chi}}{\partial y}\frac{\partial\bar{\chi}}{\partial z}+\frac{W_oW_o}{2}\frac{\partial\bar{\chi}}{\partial z}^2\right)}=\frac{-\overline{\mathbf{V}'\chi'}\cdot\nabla\bar{\chi}}{\nabla\bar{\chi}\cdot\mathbb{K}_s\cdot\nabla\bar{\chi}} \tag{30}$$

and

$$\psi_o=\frac{-\bar{\rho}\overline{v'\chi'}\left(\frac{V_oW_o}{2}\cos\phi_o\frac{\partial\bar{\chi}}{\partial y}+\frac{W_oW_o}{2}\frac{\partial\bar{\chi}}{\partial z}\right)+\bar{\rho}\overline{w'\chi'}\left(\frac{V_oW_o}{2}\cos\phi_o\frac{\partial\bar{\chi}}{\partial z}+\frac{V_oV_o}{2}\frac{\partial\bar{\chi}}{\partial y}\right)}{\nabla\bar{\chi}\cdot\mathbb{K}_s\cdot\nabla\bar{\chi}} \tag{31}$$

where $\mathbb{K}_s$ is the symmetric deviatory velocity tensor defined by (10) and (29). It is analogous to the Reynold's stress tensor, the latter being defined for temporal rather than zonal averaging.

Equations (27) to (31) have many interesting implications.

1. A solution exists unless $\nabla\bar{\chi}\cdot\mathbb{K}_s\cdot\nabla\bar{\chi}$ goes to zero faster than the numerator of (30) and (31). When integrated over the entire atmosphere this scalar product must be greater than zero because it equals $-\frac{\partial}{\partial t}\left(\frac{\bar{\chi}^2}{2}\right)$, which must be positive as $\bar{\chi}^2$ decreases towards its minimum, a uniform distribution. It may, however, be very small or slightly negative at some latitude or height and, if so, a lower limit

on the denominator must be used to maintain computational stability.

2. The numerator of (3) is the same as the common denominator for Mahlman's K_{yy}, K_{yz} and K_{zz} coefficients. Because $-\overline{V'\chi'}\cdot\nabla\bar{\chi}$ appears in the numerator instead of the denominator, the effect of a deviatory flux being approximately orthogonal to $\nabla\bar{\chi}$ apparently is not serious. Also, there appears to be no inherent difficulty with an upgradient flux ($\overline{V'\chi'}\cdot\nabla\bar{\chi} > 0$) providing that the divergence of the antisymmetric tensor compensates for its local concentrating tendency.

3. Reed and German's (1965) approximation is included also in (27) and (29) as the limiting case $\omega_0 \to 0$ for a finite τ_0. This result is obtained from (22) by dividing Φ_1 and Φ_2 by ω_0 and passing to the limit. Then

$$-\bar{\rho}\overline{V'\chi'} = \bar{\rho}K_s\tau_0\cdot\nabla\bar{\chi} \qquad (32)$$

The same result is obtained by setting $\omega_0 = 0$ in (23) which yields $Y' = V_0\cos\phi_1 t$ and $Z' = W_0\cos\phi_2 t$ and then evaluating (20) with these linear displacements. Obviously this limiting result is unrealistic for the atmosphere but, of course, one need not pass to the limit for realistic applications of their approximation. Whenever the mixing period τ_0 is small compared to the oscillatory period associated with ω_0 the approximation is reasonably valid despite the prevalence of elliptical polarizations. From this viewpoint, it is a more general approximation than Mahlman's, but because both methods eliminate ψ_0 there is reason to question their general applicability.

4. Adapting Matsuno's (1980) concept of a mixing time τ provides the additional insight that the mixing length hypothesis can be applied

to 2-D models, but the vector displacements must be corrected for elliptically polarized wave motions. In other words, the history of the air parcel's trajectory is important unless the effective mixing time is very small compared to the effective wave period. This correction for the parcel's history is reminiscent of that required for elastic collisions in molecular diffusion (Jeans, 1925).

5. Equation (27) may also resolve the perplexing results obtained by Louis (1974)[3]. Reference to (22) shows that $\Phi_1 = \Phi_2 = \frac{1}{2}$ when $\omega_o \tau_o = 1$. If, as indicated by Matsuno (1980), ψ_o does tend to cancel $\bar{\psi}$ then both the Eulerian mean circulations and the effects of the symmetric tensor would be reduced by approximately 50%. On the other hand, in the middle and upper stratosphere, where the diabatic forcing increases in magnitude, $\bar{\Psi}$ could dominate and perhaps be reinforced rather than opposed by the deviatory advections (see next section).
6. If τ becomes very small due to photochemical processes, both Φ_1 and $\Phi_2 \rightarrow 0$. Then the local change in a trace species is comparatively insensitive to transport. However, other than a loss of computer efficiency, there appears to be no logical difficulty in maintaining the transport computations. In principle, it seems preferable to do so and to consider only mixing processes in evaluating τ_o, relying on proper descriptions of the chemical sources and sinks to account for the chemical lifetimes.

PHYSICAL SIGNIFICANCE OF THE DIVERGENCE OF THE TRANSPORT TENSOR

In the above discussion we have considered mainly the properties of the asymmetric tensor and how its components could be determined from a representative three-dimensional data set. However, in a 2-D model it is the divergence

[3] Ibid.

of the tensorial product that determines the net contribution by transport process to the local time rate of change, therefore, the spatial gradients of the tensor's components are possibly as important as the components themselves. In particular, differences in the effects of the spatial gradients perhaps could explain why similar results are obtained from models whose diffusion coefficients differ drastically in magnitude.

To clarify the physical significance of the divergence of the tensor product we will first write the flux in its general form

$$-\bar{\rho}(\bar{V}\bar{\chi}+\overline{V'\chi'}) = \bar{\rho}\begin{bmatrix} K^*_{yy} & K^*_{yz} \\ K^*_{zy} & K^*_{zz} \end{bmatrix}\cdot\nabla\bar{\chi} = \bar{\rho}\mathbb{K}^*\cdot\nabla\bar{\chi} \qquad (33)$$

where $K^*_{yz}=K_{yz}+\frac{\bar{\psi}}{\bar{\rho}}$, $K^*_{zy}=K_{yz}-\frac{\bar{\psi}}{\bar{\rho}}$ and $\psi=\bar{\psi}+\psi_o$. Then the divergence of (33) can be written as

$$\nabla\cdot\left[\bar{\rho}\bar{V}\bar{\chi}+\bar{\rho}\overline{V'\chi'}\right] = -\left[\nabla\cdot\bar{\rho}K^*\right]\cdot\nabla\bar{\chi} - \left[\bar{\rho}K^*\cdot\nabla\right]\cdot\nabla\bar{\chi} \qquad (34)$$

In this form, the first term on the right represents an advection and the second a diffusion of $\bar{\chi}$, with both processes being weighted by the mean density. Thus, for example, if $\bar{\rho}$ were constant the divergence of K^* would describe an equivalent advection velocity which would include the rotational mean velocity $\bar{V}$ and an irrotational velocity associated with the deformations and divergence of the deviatory motions.

If, for simplicity of notation, we expand (34) in cartesian y,z coordinates, the two terms including the density weighting can be identified as

$$\text{advective} = -\left[\frac{\partial}{\partial y}(\bar{\rho}K^*_{yy})+\frac{\partial}{\partial z}(\bar{\rho}K^*_{zy})\right]\frac{\partial\bar{\chi}}{\partial y} - \left[\frac{\partial}{\partial y}(\bar{\rho}K^*_{yz})+\frac{\partial}{\partial z}(\bar{\rho}K^*_{zz})\right]\frac{\partial\bar{\chi}}{\partial z} \qquad (35)$$

$$\text{diffusive} = -\bar{\rho}\left[K^*_{yy}\frac{\partial^2\bar{\chi}}{\partial y^2} + \left(K^*_{yz}+K^*_{zy}\right)\frac{\partial^2\bar{\chi}}{\partial y\partial z} + K^*_{zz}\frac{\partial^2\bar{\chi}}{\partial z^2}\right] \tag{36}$$

It is now clear from (36) that the stream function ψ will cancel in the central term, therefore, only the symmetric tensor contributes to the simulated diffusion, but from (35) one can see that both antisymmetric and symmetric tensors contribute to the advection. In consideration of this dual role it seems appropriate to call K^* a "transport" rather than a "diffusion" tensor.

Also, from (35) after the stream functions and the expression (29) for the symmetric tensor are introduced, the effective meridional advection velocity

$$V_{eff} = \bar{V} + V_S - \frac{1}{\bar{\rho}}\left[\frac{\partial}{\partial y}\left(T_1\bar{\rho}\frac{V_0V_0}{2}\right) + \frac{\partial}{\partial Z}\left(T_1\bar{\rho}\frac{V_0W_0}{2}\cos\phi_0\right)\right] \tag{37}$$

and vertical advection velocity

$$W_{eff} = \bar{W} + W_S - \frac{1}{\bar{\rho}}\left[\frac{\partial}{\partial Z}\left(T_1\bar{\rho}\frac{W_0W_0}{2}\right) + \frac{\partial}{\partial y}\left(T_1\bar{\rho}\frac{V_0W_0}{2}\cos\phi_0\right)\right] \tag{38}$$

Here, to refresh one's memory, $\bar{v}$ and $\bar{w}$ are the Eulerian mean velocities, computed directly from the gridpoint values of v and w, while v_s and w_s symbolize the mean velocities attributed to Stokes drift, those derived from gradients of ψ_0. Presumably the latter velocities will have signs opposite to the former and, therefore, act to reduce the Eulerian mean circulations. However, (35) - (38) clearly imply that the divergence of the symmetric tensor can also effectively augment or oppose the advection by Eulerian mean motions.

Furthermore, although (37) and (38) contain many variables, some of the dominant terms can be easily deduced and interpreted. For example, when $\frac{\partial T_1}{\partial y}$ is small, the meridional gradient of deviatory kinetic energy density will produce advections that are directed away from the energy density maximum. Since the low wave numbers dominate the energy density, they are mainly responsible for the meridional deviatory advection. Also, in the tropics, where w_o and $\cos \phi_o$ are probably small, the vertical gradient of the vertical deviatory kinetic energy density can modify the vertical advection. Thus, the amplitudes of Kelvin and gravity modified Rossby waves become important to tropospheric-stratosheric exchange.

Finally, both the advective and diffusive effects of the complete spectrum of internal waves depends directly on T_1. If T_1 is small, these irreversible effects are negligible and the wave transports are essentially reversible. Since T_1 is small when the product $\omega_o \tau_o$ is large, the effective mixing time τ_o plays a critical role in the parameterizations. It is difficult to estimate the magnitude and the spatial gradients of τ_o. On the basis of the measurements of strontium 89 and barium 140, products of the first French nuclear bomb test in the Sahara, Danielsen et al., (1962)[5] deduced a value of the order of a few days. A similar range of values was deduced from the dilution of strontium 90 and potential vorticity during Project Springfield (Danielsen, 1968). However, Staley (1957) and more recently Shapiro (1978) have estimated smaller values, approaching the order of half-a-day. Certainly, in regions of wave induced turbulence or cumulonimbus entrainment, the mixing times can be of the order of minutes. Since the effective τ_o can be computed from T_1 and ψ_o, it will be interesting to see what values are obtained from this objective method.

In any case, it is intuitively satisfying to discover from the method that

[5] Ibid.

the large-scale waves are predominantly responsible for transport potentials, through their amplitudes and realtive phases of meridional and vertical velocities, while the small-scale waves, which are more directly responsible for irreversible mixing, control τ, and, therefore, the realization of transport potentials.

SUMMARY

With the growing interest in and development of zonally averaged models, there is a corroborative need for an objective, statistical description of the fully three-dimensional transports. In general, these models will be based on Eulerian coordinates. The major disadvantage of averaging over fixed spatial coordinates is that the grid volumes represent completely open systems. Thus, integrals which extend over all longitudes completely eliminate all non-zero Fourier wave modes. That is, transport by the complete wave spectrum must be described statistically.

On the other hand, it is shown that Lagrangian integrals suffer from a much more serious difficulty. Data limitations preclude completely closed systems, but they can be partially closed, i.e., closed to all resolvable scales of motion. However, then the boundaries of the system deform, twist and fold. The deformations start with large-scale motions and proceed intermittantly to smaller and smaller scales. Consequently, either the boundary is difficult to locate or the deviatory fluxes across the boundary are difficult to objectively determine.

A major advantage of the Eulerian average is that the local change in $\bar{\chi}$ due to transport reduces to two terms, $\nabla\cdot\left(\bar{\rho}\bar{V}\bar{\chi}+\bar{\rho}\overline{V'\chi'}\right)$, the convergence of the mean flux and of the mean of the deviatory flux, which can be objectively determined from representative meteorological data. If the velocity and χ are ex-

panded in a Fourier series, the products of wave number zero determine the mean flux and the mean of the deviatory flux reduces to the sum of the products for each nonzero wave number. All products between nonequal wave numbers vanish.

Taking advantage of this orthonormal property, the density weighted, deviatory velocity tensor $\bar{\rho}\overline{V'V'}$ can be expressed in terms of an effective ellipse whose major axis squared is the mean kinetic energy density of the meridional deviations and whose minor axis squared is the mean kinetic energy density of the vertical velocity deviations multiplied by the sine of the mean phase angle ϕ_o between v' and w'. Also, the slope of the major axis is proportional to the cosine of the same angle ϕ_o.

This analysis method applied to velocity data from the GFDL's GCM demonstrates that the slopes of the major axes are negative in the cyclonic middle and lower stratosphere, in support of Newell's (1964) interpretation of a counter-gradient transport for ozone and heat. The same analyses show that elliptical polarization is characteristic of the small wave number modes, those which have the largest amplitudes, and that the amplitudes vary with latitude, so that a contribution to the mean circulations by Stokes drift is probable. As shown by Matsuno (1980) this contribution would appear as an antisymmetric tensor in the statistical description of the transports.

The symmetric part of the tensor is essentially the product of the density, a time constant, and the Reynold's stress tensor. The antisymmetric parts include the stream functions for the mean circulations and for contributions due to Stokes drift.

To evaluate the components of these tensors requires a representative set of u,v and w velocity components and an appropriately balanced set of thermodynamic variables to permit representative computations of potential vorticity.

Given such a set, either from numerical diagnostic or predictive analyses,a method for reducing the problem to two equations and two unknowns is presented and discussed. Work has begun to analyze both types of data to obtain solutions, twice daily or four times daily. Later these solutions will be temporally averaged.

The asymmetric tensor has been called simply a transport tensor because the divergence of the tensor-vector inner product includes both advection and diffusion of $\overline{\chi}$. Of course, it includes advection by the mean $\overline{V}$ velocities, the rotational velocities, but it includes also advections by irrotational deviatory velocities. Thus, for example, important advections result from spatial gradients of the deviatory kinetic energy density.

In the absence of the essential data set there are a large number of degrees of freedom for tuning a model's transport coefficients. Consequently, the current lack of unanimity among 2-D modelers relative to transport specifications is understandable. However, for a generally valid set, applicable to many tracers, the degrees of freedom should be effectively eliminated as the data sets are generated and processed.

ACKNOWLEDGMENTS

The authors express gratitude to D. Deaven and P. Swan for developing computer programs essential to this work, and to J. Mahlman for making data available. They also thank those named above and L. Pfister, for many stimulating discussions and helpful criticisms.

REFERENCES

Brewer, A. W., Evidence for a world circulation provided by measurements of helium and water vapor distribution in the stratosphere, Qtly. J. Roy. Met. Soc., 75, 351-363, 1949.

Danielsen, E. F., Trajectories: Isobaric, isentropic and actual, J. Meterol., 18, 479-486, 1961.

Danielsen, E. F., Stratospheric-tropospheric exchange based on radioactivity, ozone and potential vorticity, J. Atmos. Sci., 25, 502-518, 1968.

Danielsen, E. F. and J. F. Louis, Transport in the stratosphere, in The upper atmosphere and magnetosphere, Ch 9, National Research Council's Studies in Geophysics, 1977.

Danielsen, E. F. and R. S. Hipskind, Stratospheric-tropospheric exchange at polar latitudes in summer, J. Geophys. Res., 85, 393-400, 1980.

Davidson, B., J. P. Friend and H. Seits, Numerical models of diffusion and rainout of stratospheric radioactive materials, Tellus, 18, 301-315, 1966.

Dobson, G. M. B., Origin and distribution of the polyatomic molecules in the atmosphere, Proc. Roy. Soc., Ser. A, Vol. 236, No. 1205, 187-192, 1956.

Eady, E. T., Long waves and cyclone waves, Tellus, Vol. 1, No. 3, 33-52, 1949.

Fleagle, Robert G., Instability criteria and growth of baroclinic disturbances, Tellus VIII, 168-176, 1955.

Fleagle, Robert G., On the dynamics of the general circulation, Qtly. J. Roy. Met. Soc., 83, 1-20, 1957.

Fultz, D. and H. Riehl, Jet stream and long waves in a steady rotating-dishpan experiment, Qtly. J. Roy. Met. Soc., 83, 215-231, 1957.

Green, J. S. A., Transfer properties of the large-scale eddies and the general circulation of the atmosphere, Qtly. J. Roy. Met. Soc., 96, 157-185, 1970.

Jeans, J. H., The dynamical theory of gases, Dover Press, New York, N.Y., 1925.

Kuo, H. L., Forced and free meridional circulations in the atmosphere, J. Met., 13, 561-568, 1956.

Krishnamurti, T. N., The subtropical jet stream of winter, J. Meteor., 18, 172-191, 1961.

Mahlman, J. D., On the maintenance of the polar front jet stream, J. Atmos. Sci., 30, 544-557, 1973.

Matsuno, T., Lagrangian motion of air parcels in the stratosphere in the presence of planetary waves, Pure and Appl. Geophys., 118, 189-216, 1980.

Newell, R. E., The transport of trace substances in the atmosphere and their implications for the general circulation of the stratosphere, Geofisica Pura e Applicata, 49, 137-158, 1961.

Newell, R. E., The circulation of the upper atmosphere, Scientific American, 210, 62-74, 1964.

Reed, R. J. and K. E. German, A contribution to the problem of stratospheric diffusion by large-scale mixing, Mon. Wea. Rev., 93, 313-321, 1965.

Shapiro, M. A., Further evidence of the mesoscale and turbulent structure of upper level jet stream-frontal zone systems, Mon. Wea. Rev., 106(8), 1110-1111, 1978.

Sommerfeld, A., Mechanics of deformable bodies, Academic Press, New York, N.Y., 1950.

Staley, D. O., A study of tropopause formation, Beitr. Phys. Atmos., 29(S), 290-316, 1957.

Stewart, H. J., Kinematics and dynamics of fluid flow, Sect. VI, Handbook of Meteorology, McGraw-Hill Book Co., New York, N.Y., 1945.

Wallace, J. M., Trajectory slopes, countergradient heat fluxes and mixing by lower stratospheric waves, J. Atmos. Sci., 35, 554-558, 1978.

Wolf, O. R., The distribution of atmospheric ozone, Proceedings, 8th American Scientific Congress, Vol. 7, 439-446, 1942.

APPENDIX I

A generalization of Leibnitz' formula for transforming from the time derivative of a moving integral to the integral of a partial time derivative can be written in the following form:

$$\frac{D}{Dt}\int \chi\, dV \equiv \left(\frac{\partial}{\partial t} + \mathbf{V}_s\cdot\nabla\right)\int \chi\, dV = \int \frac{\partial \chi}{\partial t}\, dV + \oint \mathbf{V}_B \chi \cdot d\mathbf{A} \qquad (1.1)$$

where $\mathbf{V}_s$ is the velocity of the bulk system, $\mathbf{V}_B$ is the local velocity of its boundary and dV and d$\mathbf{A}$ are its differential volume and surface area, respectively.

For Eulerian integrals, $\mathbf{V}_s$ and $\mathbf{V}_B$ = 0, therefore, the bulk systems are stationary, completely open systems of constant volume. The conservation equations for mass, momentum and energy density can be integrated over the volume to yield the appropriate bulk equations.

For Lagrangian integrals the total or bulk mass is constant, but there are two possible solutions. If $\chi = \rho$ substitution of the mass conservation equation into (1.1) yields

$$\frac{DM}{Dt} = -\oint (\mathbf{V}-\mathbf{V}_B)\rho \cdot d\mathbf{A} = 0 \qquad (1.2)$$

If $\mathbf{V} \equiv \mathbf{V}_B$ the system is closed for all but the molecular motions, but it is physically impossible to determine the three-dimensional velocities of the boundary. An alternative approach is to set $\mathbf{V}_B = \overline{\mathbf{V}}$, a continuous function of the spatial coordinates, where $\overline{\mathbf{V}}$ is the density weighted mean for the bulk volume

$$\overline{\mathbf{V}} = \frac{\int \rho \mathbf{V}\, dV}{\int \rho\, dV} \qquad (1.3)$$

Then with $\mathbf{V} = \bar{\mathbf{V}} + \mathbf{V}'$ equation (1.2) becomes

$$\frac{DM}{Dt} = -\oint \mathbf{V}'\rho \cdot d\mathbf{A} = -\int \nabla \cdot \rho \mathbf{V}' dV = -\nabla \cdot \int \rho \mathbf{V}' dV = 0 \tag{1.4}$$

In this case the system moves with the velocity of its center of mass, remains contant in mass, but is open for all scales of motion smaller than that defined by the averaging volume. Thus, for example, the bulk or mean momentum equations are, for the Eulerian integrals

$$\frac{\partial \bar{\mathbf{V}}}{\partial t} + \bar{\mathbf{V}} \cdot \nabla \bar{\mathbf{V}} = -\frac{\nabla \bar{p}}{\bar{\rho}} - g - \bar{f} k \times \bar{\mathbf{V}} - \frac{\nabla}{\bar{\rho}} \cdot \left[\bar{\rho} \overline{\mathbf{V}'\mathbf{V}'} + \bar{\sigma} \right] \tag{1.5}$$

and for Lagrangian integrals

$$\frac{D\bar{\mathbf{V}}}{Dt} = -\frac{\nabla p}{\bar{\rho}} - g - f k \times \bar{\mathbf{V}} - \frac{\nabla}{\bar{\rho}} \cdot \left[\rho \overline{\mathbf{V}'\mathbf{V}'} + \bar{\sigma} \right] \tag{1.6}$$

where p, g and f are the pressure, vector acceleration of gravity and the vertical component of the earth's vorticity, and σ is the molecular stress tensor.

Equations (1.5) and (1.6) are equivalent in the sense that to follow the bulk systems one needs to know the spatial, temporal distributions of $\bar{\mathbf{V}}$ and, in general, the correlations between the deviatory velocities, although different for the two systems, remain unknowns.

PART II

NUMERICAL DIAGNOSTIC METHOD

INTRODUCTION

As discussed earlier, the atmosphere's asymmetry prevents direct measurements of both the important vertical velocities and the ageostrophic horizontal velocities which generate them. We have no alternative but to compute them from the basic hydrodynamic equations using the available, incomplete and partially distorted observations. A reliable analysis method must compensate for these two data deficiencies and also produce representative vertical velocities. Because the radiosonde and rawinsonde stations are mainly located on the large continents, the data density over the oceanic regions is too low to permit use of most analysis methods. Instead, special techniques which utilize time continuity are necessary for hemispheric or global analyses.

In hand analysis methods, time continuity charts are used to extend the analyses over the oceans. One relies on the principle that the lifetime of the large-scale features is longer than the transit time between adjacent stations and one uses pattern recognition to identify and adjust the features on the individual analyses. These techniques can be used to test objective numerical methods but they are difficult to simulate by computer algorithms.

Instead, we take advantage of the constant pressure analyses produced by the National Oceanographic and Atmospheric Administration's Numerical Meteorological Center (NMC), and available on tapes at the National Center for Atmospheric Research. These rectangular i,j gridpoint analyses of geopotential height and temperature are a blend between numerical predictions and observations, thus time continuity is imposed by the dynamics of the numerical prediction model and adjustments are made when the observations indicate that there are systemmatic errors in the predicted patterns.

Direct comparisons of the NMC analyses with hand analyses indicated that they were usually good at mid and high latitudes, but often contained spurious

cyclones and anticyclones at low latitudes. These results are reasonable because the low latitudes have the largest data gaps, the poorest data density. Nevertheless, it was necessary to eliminate them and special techniques were developed to do this objectively. Of course, there is no substitute for data and, therefore, the results are least accurate at low latitudes. In particular, the tendency will be to suppress variability in these regions by relying more on monthly means than synoptic values of height, temperature, moisture and wind components. Computations of the variability at the individual radiosonde stations support this philosophy. The tropical stations have the smallest variability.

GENERAL OBJECTIVES OF THE METHODS

The primary objective of the diagnostic method is to derive representative, dynamically balanced, ageostrophic winds, vertical velocities and thermodynamic scalars at a uniformly spaced grid over the northern hemisphere. All computations are made in isentropic rather than isobaric surfaces to take advantage of the isentropic constraint as a reasonably accurate first approximation to reality. This constraint decouples the individual entropy surfaces permitting each surface to be treated separately. After these analyses are completed, the isentropic constraint will be relaxed and the complete set of isentropic surfaces will be linked by solving Poisson type equations in three dimensions. The discussion here will be limited to the isentropic approximation.

Decoupling the solutions is a distinct advantage because the three-dimensional velocities are reduced to two horizontal components in the coordinate surfaces plus the vertical velocity of the surfaces. The latter can be derived from the horizontal velocities and the thermodynamic variables.

Therefore, we can derive a stream function and velocity potential describing the ageostrophic winds from the Montgomery stream function on each entropy surface by solving Poisson type equations in two rather than three dimensions.

An iterative method is used to first compute a stream function from the geostrophic vorticity, then the vorticity equation is solved for a generalized velocity potential, whose Laplacian includes the advection of vorticity by the divergent wind plus the vorticity weighted divergence on the entropy surfaces. After solving for the divergent wind components, the balance equation is solved for a new stream function which now includes super- and subgeostrophic rotational components. Then, finally, using this stream function the vorticity equation is resolved for a new generalized velocity potential.

In these computations successive gridpoint analyses are used to evaluate the local time derivatives. Since the data are available at 12 hr intervals a central 24 hr difference is used. This time differencing is equivalent to applying a temporal filter which completely eliminates all waves with periods ≤ 1 day. We would prefer to have data every 6 hrs, but consider temporal filtering much better than spatial filtering for our purposes.

Being interested in atmospheric transport, especially stratospheric-tropospheric exchange, we know from previous tests that spatial filtering in isobaric coordinates tends to suppress or eliminate the strongly asymmetrical structures associated with tropopause folding. On the other hand, temporal filtering in isentropic coordinates does not eliminate these structures because their lifetimes are of the order of several days and the asymmetry is mainly due to large gradients orthogonal to the entropy surfaces. Thus, use of isentropic coordinates provides the additional advantage of retaining higher order spatial resolution when the solutions are transformed to x,y,z space.

After the stream function and velocity potential are determined, the

equations of horizontal motion are solved for a new Montgomery stream function. This step assures that the thermodynamic scalar fields are dynamically consistent with the wind fields and with the temporal filtering.

Having determined a new Montgomery stream function, ψ_M, we know the specific energy on each entropy surface but not how it is partitioned. Since

$$\psi_M = c_p T_v + gz \tag{2.1}$$

is the sum of the enthalpy and the geopotential energy per gram, we need to separately determine the two specific energies. In (2.1) c_p is the specific heat at constant pressure, T_v is the virtual temperature, g is the acceleration of gravity and z is the height of the θ_v surface.

To separate them we differentiate the ψ_M solutions at each gridpoint by the logarithm of the equivalent potential temperature, i.e.,

$$\frac{\partial \psi_M}{\partial \ln \theta_v} = c_p T_v \tag{2.2}$$

Then it is a simple matter to determine z, the height of the θ_v surface and, finally, from the total derivative to determine the adiabatic vertical velocity W_{ad}. This completes the analysis method for the primary variables and permits a direct computation of the quasi-conservative scalar variable, the potential vorticity.

The potential vorticity, defined by

$$S = \alpha \nabla \theta_v \cdot \left[\nabla \times \mathbf{V} + 2\Omega \right] \tag{2.3}$$

can be expanded in x,y,z coordinates, as

$$S = \alpha \frac{\partial \theta_v}{\partial x}\left(\frac{\partial w}{\partial y} - \frac{\partial v}{\partial z}\right) + \alpha \frac{\partial \theta_v}{\partial y}\left(\frac{\partial u}{\partial z} - \frac{\partial w}{\partial x} + \lambda\right) + \alpha \frac{\partial \theta_v}{\partial z}\left(\frac{\partial v}{\partial x} - \frac{\partial u}{\partial y} + f\right) \quad (2.4)$$

$$10^3\ 10^{-6}\left(10^{-6}\ \ 10^{-2}\right)\quad 10^3\ 10^{-6}\left(10^{-2}\ \ 10^{-6}\ \ 10^{-4}\right)\quad 10^3\ 10^{-4}\left(10^{-4}\ \ 10^{-4}\ \ 10^{-4}\right)$$

where α is the specific volume and f, λ are the vertical, horizontal components of 2Ω, the earth's vorticity. Retaining the dominant terms, we reduce this to

$$S = \alpha \frac{\partial \theta_v}{\partial z}\left[\left(\frac{\partial v}{\partial x} + \frac{\partial v}{\partial z}\frac{\partial z}{\partial x}\bigg|_\theta\right) - \left(\frac{\partial u}{\partial y} + \frac{\partial u}{\partial z}\frac{\partial z}{\partial y}\bigg|_\theta\right) + f\right] \quad (2.5)$$

which is identical to

$$S = \alpha \frac{\partial \theta_v}{\partial z}\left(\frac{\partial v}{\partial x}_\theta - \frac{\partial u}{\partial y}_\theta + f\right) = \alpha \frac{\partial \theta}{\partial z}\left(\zeta_\theta + f\right) \quad (2.6)$$

It is important to recognize that the potential vorticity is quasi-conservative only if it is defined by (2.3) to (2.6). When ζ_θ is replaced by ζ_p, as many authors do, it is not conserved even for isentropic processes. Here we want to use S as a tracer for stratospheric air, so it is relevant to determine the proper quantity. In this work, ζ_θ is obtained directly from the Laplacian of the stream function since an isentropic surface is also a constant θ_v surface.

SPECIFIC DETAILS OF THE METHOD

At each NMC gridpoint we use the z and T_v values versus p to construct a sounding from which ψ_M is computed, as described in Danielsen and Deaven (1974). This grid is cartesian on a polar stereographic projection, true at 60^oN.

However, for our computations it is much more convenient to use a spherical polar grid so we must convert from x,y to ϕ,λ where ϕ is the latitude angle and λ is the longitude angle.

Originally a double parabolic method was used to interpolate to the ϕ,λ points, but this method was discovered to generate vorticity which tended to amplify in the numerical solutions. To eliminate spurious vorticities, a 5th order interpolation function in x and y was developed and tested. The test used an analytic function generated from Fourier components to simulate a reasonably realistic stream function. From the values computed at the x,y gridpoints, values were interpolated to the ϕ,λ points and then compared to the exact values at the same ϕ,λ points. Interpolation errors were evaluated for 1st, 3rd and 5th order in x and y. The reduction in error was significant, justifying use of the 5th order functions.

After interpolating ψ_M to the ϕ,λ gridpoints, which includes 32 intervals in latitude and 128 in longitude (both powers of 2 for later use of Fast Fourier Transform) the analyses are extended to the equator by merging the synoptic solutions south of 30°N latitude with the monthly mean values. The method used to compute and analyze the monthly means will be discussed later.

The first step in the diagnostic method is to solve for a stream function whose Laplacian equals the geostrophic vorticity obtained from ψ_M,

$$\nabla^2\psi_1 = \frac{\nabla^2\psi_M}{f} - \frac{1}{fR}\frac{\partial\psi_M}{\partial\phi}\frac{1}{R}\frac{\partial}{\partial\phi}(\ln f) \qquad (2.7)$$

In solving (2.7) a spherical, polar Poisson solver is used which requires a value of ψ_1 at the pole and at the equator. To determine appropriate boundary values (2.7) is integrated over the polar area from the pole to the successive values of ϕ. In each integration, use is made of Stokes theorem to convert the

area to a line integral which determines the appropriate mean zonal wind at each ϕ gridline. At the equator, the zonal, monthly mean value is imposed. Then the integration of $\frac{\partial \bar{\psi}_1}{\partial \phi}$ over all latitudes is made to determine the proper pole value to be associated with the equatorial value, use being made of L'Hospital's rule to determine the correct 2nd derivative with respect to ϕ at the equator.

Having determined ψ_1, the first approximation to the velocity is given by

$$\mathbf{V}_1 = \mathbf{r}_1 \times \nabla \psi_1 \tag{2.8}$$

where $\mathbf{r}_1$ is a unit radial (vertical) vector. $\mathbf{V}_1$ closely resembles the geostrophic velocity but it is nondivergent.

To obtain a second approximation, the vorticity equation

$$\frac{\partial}{\partial t}\left(\nabla^2 \psi_1\right) + \left(\mathbf{r}_1 \times \nabla \psi_1\right) \cdot \nabla \left(\nabla^2 \psi_1 + f\right) = -\nabla^2 \Phi_2 \tag{2.9}$$

is solved for Φ_2. Here use is made of Gauss' Thorem to convert the area integral of the divergence of $\nabla \Phi_2$ to a line integral which determines the mean meridional wind for each ϕ gridline. At the equator this mean wind is set equal to zero, to be consistent with the adiabatic approximation. Again, the ϕ integration is performed to obtain Φ_2 at the pole when $\Phi_2 = 0$ at the equator.

With Φ_2 evaluated at each gridpoint, we have to compute the divergent velocity by solving

$$\mathbf{V}_d \left(\nabla^2 \psi_1 + f\right) = \nabla \Phi_2 \tag{2.10}$$

Clearly this solution will be unstable when the absolute geostrophic vorticity is small. To date we have found it necessary to impose a lower limit of 10^{-5}sec^{-1} to avoid excessive divergent velocity components. This limit is

reached by smoothing or averaging with the larger surrounding values, thus it is the numerical equivalent to the mixing which develops from inertial instability. So the second approximation to the velocity

$$\mathbf{V}_2 = \mathbf{V}_1 + \mathbf{V}_d = \mathbf{r}_1 \times \nabla\psi_1 + \frac{\nabla\Phi_2}{\nabla^2\psi_1 + f} \tag{2.11}$$

The next step involves substituting $\mathbf{V}_2$ into a generalized Balance Equation which is obtained by neglecting only the time derivative of the divergence,

$$\nabla^2\psi_3 = -f + \sqrt{f^2 + 2f\zeta_g + div^2 + def^2 + \frac{u^2+v^2}{r^2}} \tag{2.12}$$

Here again, Stokes Theorem is used to determine the boundary conditions. Then the 3rd approximation is

$$\mathbf{V}_3 = \mathbf{r}_1 \times \nabla\psi_3 + \frac{\nabla\Phi_2}{\nabla^2\psi_1 + f} \tag{2.13}$$

Now (2.9) is resolved with the new stream function ψ_3 to determine a new velocity potential Φ_4, so the final velocity approximation is

$$\mathbf{V}_4 = \mathbf{r}_1 \times \nabla\psi_3 + \frac{\nabla\Phi_4}{\nabla^2\psi_3 + f} \tag{2.14}$$

In the first solution of (2.9) three successive analyses of ψ_1 are required. In the second solution, three successive analyses of ψ_3 are required which, in turn, depends on five successive analyses of ψ_1.

A comparison of the ψ_3 and ψ_1 fields indicates a proper qualitative adjustment for subgeostrophic speeds in troughs and supergeostrophis speeds in ridges. Also, a comparison of the divergence patterns from Φ_4 and Φ_2 indicates

computational stability because the patterns are basically similar in the location of the convergent and divergent cells with only minor adjustments in the patterns.

MONTHLY MEAN COMPUTATIONAL METHODS

These initial tests were made by merging the transformed NMC analyses with hand drawn analyses at low latitudes. A direct comparison of the observed winds with the NMC winds showed major discrepancies at low latitudes due to the presence of small cyclones and anticyclones in the NMC analyses. Obviously, these spurious vortices must be eliminated but by objective rather than hand methods. After completing the processing of digitally recorded radiosonde serial ascents from the Panama Canal Zone - sondes were released every 6 hrs and were tracked by radar - we realized that the large-scale structures were slowly varying and that the day-to-day variability was produced by internal waves which could not be resolved by the present day network. For details the reader is referred to the NASA report by Danielsen and Hipskind (1980).

On the basis of these results it seemed advisable to improve the accuracy of the tropical measurements by temporal averaging and to base the extension to the equator on monthly mean values. However, a technique for detecting and eliminating large errors and nonrepresentative data had to be developed.

A major difficulty is to discriminate between height and temperature errors in the coded data. The method we developed and tested has produced excellent results. We apply it to all radiosonde reports in the NMC radiosonde data tapes but restrict the computations to the mandatory levels only.

Starting at the lowest reported mandatory level, we compute the thickness of the next layer from the mean of the two reported temperatures and add it to the lower (first) reported height. The second reported height is then sub-

tracted from the computed height and the error is stored. Next, the thickness of the second layer is computed and added to the second reported height. Once again, the third reported height is subtracted from the computed height and this error is compared to the former error. If both errors exceed a threshold value corresponding to an error in mean temperature of $\pm 5^{o}K$ the signs of the errors are compared. When both errors have the same sign a temperature error is detected at level two. When the signs differ, a height error is detected at level two.

The most common coding and transmission errors for temperature are multiples of $10^{o}K$ or a reversal in sign, therefore, tests are made to determine whether errors of this type are responsible for the height discrepancies. If so, the temperature at the second level is corrected; if not, the temperature data are omitted from the mean.

To correct a single reported height error, i.e., when the two successive errors have opposite signs, one-half of the difference (error 2 - error 3) is subtracted from level two.

When errors are detected that do not fit this pattern, the data are omitted from the mean but flagged for a subsequent test. As part of the computation the mean, standard deviation from the mean, and the number of observations used in the mean are stored. The flagged data are then checked by computing the deviations from the mean and any deviation exceeding three standard deviations are rejected.

The winds at the standard pressure levels are first compared to a threshold which is set to 30 m sec^{-1} at 1000 mb and which increases linearly to 150 m sec^{-1} at 300 mb. At all lower pressure levels the threshold remains constant at 150 m sec^{-1}. A second check is based on wind shears, the upper acceptable limit being $5 \times 10^{-2} sec^{-1}$. If two successive shears exceed this

limit and have opposite signs the central level wind is rejected. If the limit is exceeded in only one layer the two winds are flagged for a subsequent test based on a comparison of the deviations from the mean to the standard deviations.

After all data for each month are processed, the geopotential heights will be objectively analyzed to obtain gridpoint values. Two different methods are being tested but both include a test for nonrepresentative heights and/or winds. For example, we have found examples where stations reported only a few times in a month and, although the observations are internally consistent, their means were nonrepresentative. The tests are sensitive enough to detect the same data which has been rejected by hand analyses methods.

SUMMARY

The objective diagnostic method discussed briefly above yields balanced representative ageostrophic horizontal wind components, adiabatic vertical velocities and consistent thermodynamic scalars at a uniform latitude-longitude grid over the northern hemisphere. To date the method, based on isentropic analyses, is restricted to those entropy surfaces which do not intersect the earth's surface. Methods are still being developed and tested to extend the analyses to the surface.

REFERENCES

Danielsen, E. F. and D. Deaven, Methods for deriving a two-dimensional transport model, Proceedings, 3rd Conference on the Climatic Impact Assessment Program, DOT-TSC-OST-74-15, edited by A. J. Broderick and T. M. Hard, U.S. Dept. of Trans., 83-91, 1974.

Danielsen, E. F., R. S. Hipskind and S. E. Gaines, High resolution vertical profiles of wind, temperature and humidity obtained by computer processing and digital filtering of radiosonde and radar tracking data from the ITCZ experiment of 1977, NASA Contractor Rept. 3269, Contract NAS2-10023, 116 pp., 1980.

☆ U.S. GOVERNMENT PRINTING OFFICE 1980 -341-428/370


DATE
ILME